DEPARTMENT OF COMMERCE
FREDERICK H. MUELLER, Secretary

WEATHER BUREAU
F. W. REICHELDERFER, Chief

# MONTHLY WEATHER REVIEW

JAMES E. CASKEY, JR., Editor

Volume 88
Number 5

MAY 1960

Closed July 15, 1960
Issued August 15, 1960

## WIND SPEED AND AIR FLOW PATTERNS IN THE DALLAS TORNADO OF APRIL 2, 1957

WALTER H. HOECKER, JR.

U.S. Weather Bureau, Washington, D.C.

[Manuscript received March 15, 1960; revised June 10, 1960]

### ABSTRACT

A composite distribution of tangential and upward components of air flow is determined by tracing particles of debris and cloud tag movements in scaled movies of a tornado. The greatest tangential speed measured is 170 m.p.h. and the greatest upward speed derived is 150 m.p.h. A distribution of the convergent radial component of motion in the lower 600 ft. of the vortex is synthesized and used to generate a vertical speed distribution which nearly duplicates the observed vertical speed distribution.

The observed radial distribution of the vertical component of relative vorticity at three levels is shown and convergence at the 500-ft. radius is computed using the synthesized radial speed distribution. Three-dimensional trajectories of air parcels in the lower portion of the vortex are also shown.

### 1. INTRODUCTION

For many decades the speed of the wind in the tornado has been an object of great curiosity, and many indirect means have been used to estimate at least the maximum speed near the ground in a given tornado and many theoretical studies have estimated the speed distribution in the tornado vortex. In this investigation the scaling of high-quality tornado movies (some scenes taken with a 10-times magnifying telephoto lens) has allowed the determination of derived wind speeds in the Dallas, Tex., tornado of April 2, 1957, by tracing the time rate of movement of cloud fragments and debris elements circulating around this tornado.

A limited distribution of the speeds of the tangential and vertical wind components over a range of radii and levels above the ground in the space occupied by the Dallas tornado has been derived. Of necessity, the measurements were not simultaneous, being made in several periods where the earliest and latest measurements were separated by about 19 minutes. Therefore, the speed distributions shown in this paper are composites of speeds from different times and it will be shown that speeds obtained late in the tornado lifetime do not fit the pattern of those obtained predominantly in the early part. The fact that the condensation envelope, or visible tornado, was suspended a few hundreds of feet aloft during most of this measuring period made possible some measurements in a region that ordinarily is obscured. Wind speeds quoted for the tornado are relative to the tornado, and are those of the tracer elements except where corrections have been applied to some vertical speeds. Wind speed assumptions relative to tracer speeds are explained in the text. Radial symmetry is assumed for all speed distributions described in this paper.

### 2. TANGENTIAL WIND SPEEDS

The tangential components of wind around the Dallas tornado are discussed in this section. It is to be kept in mind that the data points are located where by chance tracer particles were located and that the highest speed measured was not necessarily the highest speed existing in the tornado. It is also well to remember that this

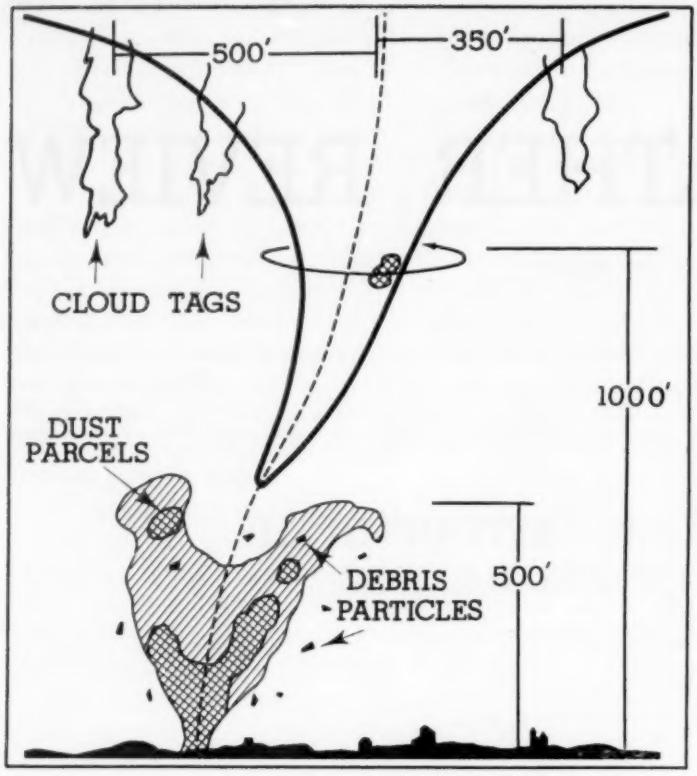


FIGURE 1.—The various types of elements used as air flow tracers in the wind speed measurements of the Dallas tornado of April 2, 1957.

tornado was relatively small, but at the same time was fairly stable in character; at the ground its damage path was at times spotty (c.f. [5]).

Figure 1 shows the various types of elements that were used as air flow tracers in measuring the speed. In the upper portion were the cloud tags and fragments rotating around the tornado; and in the lower portion, that is, in and around the debris cloud, were the dust parcels and pieces of debris. In some instances the speed of roughness elements on the surface of the funnel was measured and in one instance the speed of rotation of a flattened funnel tip was determined; both gave speeds on the funnel surface. It was assumed that the cloud elements and dust or mud-spray parcels were moving at the actual speed of the air in which they were imbedded. For the more or less solid debris particles, it was presumed that the wind speed was at least as fast as that of the particle of debris used as a tracer. The radii of the paths of the cloud tags were found by measuring the extreme left- or right-hand projected distance that the tags extended from the tornado center as they rotated around it. The radii of the paths of solid debris particles not determinable as described above, were obtained by observing their horizontal projected speed distributions relative to the center of the tornado. Trial and error fitting of observed projected speed distribution curves to a range of computed projected speed curves allowed an estimation of the radius. The tornado appeared to be in approximately the same stage of development for most of the observations.

The distribution of tangential speeds, determined as described above, is shown in figure 2 on a graph of height versus radius. Isotachs are smoothed to these data points. The average position of the condensation envelope relative to most of the data points is shown as a dot-dash line across the upper left-hand part of the graph. The center of the tornado is, of course, along the vertical scale at zero radius. The greatest derived tangential speed was 170 m.p.h., and was found at a radius of 130 ft. and an elevation of 225 ft. This does not mean that the speed was limited to 170 m.p.h., since other tracers not considered here might have indicated greater speeds. The greatest derived low-level speed was 122 m.p.h., which was found at an elevation of 70 ft. and a radius of 90 ft. Other than the fact that the tangential speed at the earth's surface is required to be zero, the distribution of speed between the ground and the level of the 122 m.p.h. datum point is not known. Unfortunately, these data are bunched in space and some interpolation has been necessary, particularly between 500 and 1000 ft. in elevation and inward from the 400-ft. radius.

For the information of the reader the data points of figure 2 are coded as to the type of element traced in obtaining the distribution of tangential speeds. The triangles indicate that solid debris particles were tracked. These were mainly some uniformly sized rectangularly shaped thin sheets of material about 4 x 8 ft. in size and were located below 500 ft. in elevation and inward from the 300-ft. radius. The dots indicate cloud tags and dust parcels and the squares show where the surface of the condensation funnel itself was used. The two stars indicate non-uniformly sized solid debris tracers.

In considering the distribution of wind speed, one must remember that this analysis is not unique and that there are groups of data, for example some of those in the region around 1000 ft. in elevation and 500 ft. in radius, which do not fit the analysis as presented here. The isotachs could be redrawn to fit some of the other data points more closely than they are fitted in this analysis. However, if one did this it would not greatly change the pattern as shown in figure 2, but only change the radii of some isotachs. The analysis shows a band of maximum speed starting at about 60 ft. in elevation and 70 ft. in radius and increasing in diameter with height such that at the 1200-ft. level the radius is about 260 ft. Possibly the maximum speed band continued downward and inward from the lowest datum point shown in figure 2. Generally, the radial distribution of tangential speed resembles that of the Rankine combined vortex where speed increases with decreasing radius to a certain radius inside of which the speed decreases linearly to zero at the center.

The observed distribution also shows the tendency for an increase in speed with elevation for the region outside of the maximum speed band. Attention is called to the

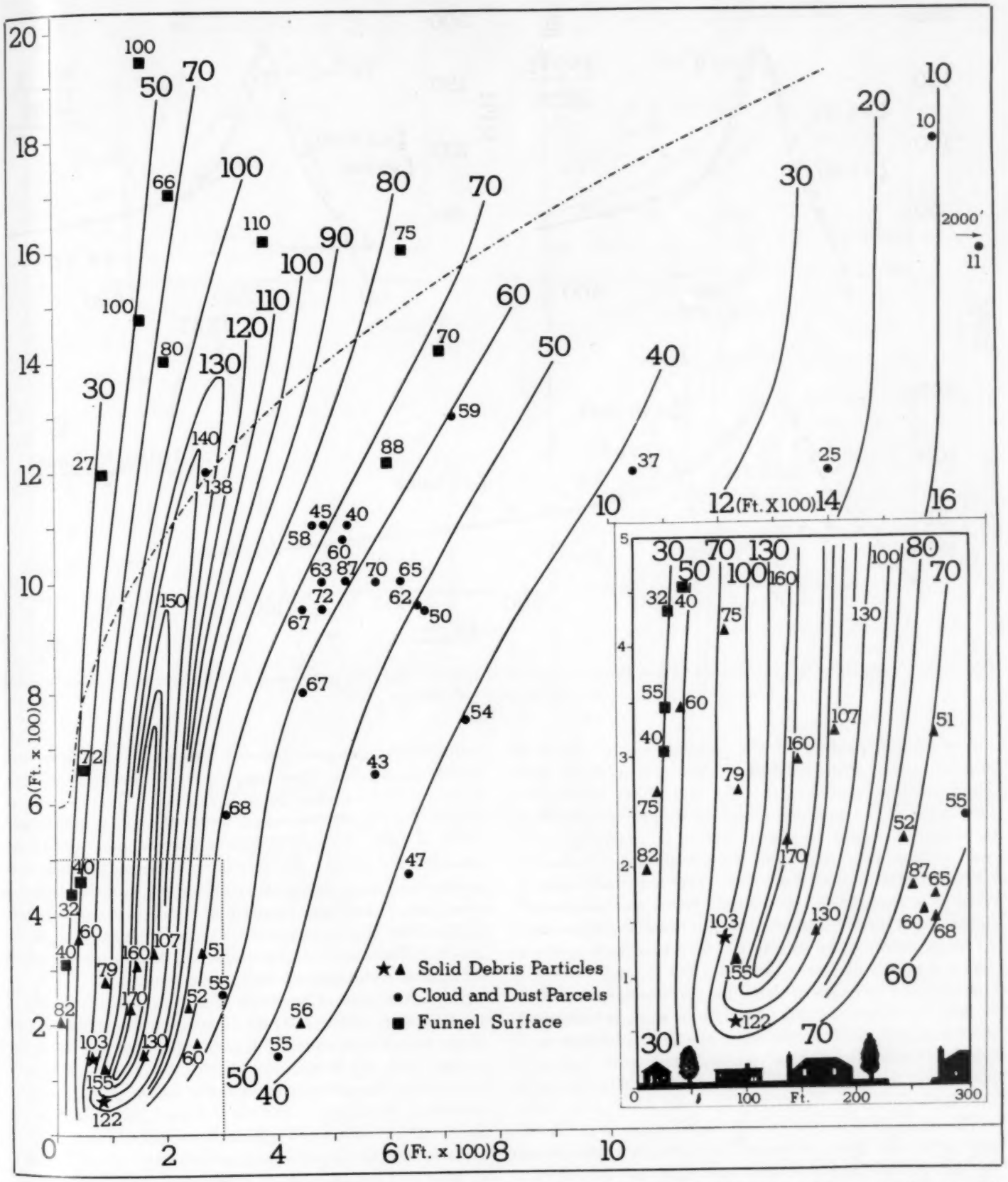


FIGURE 2.—Distribution of derived tangential speed from the center of the tornado to a radius of 2000 ft. and from near the ground to about 1800 ft. in elevation.

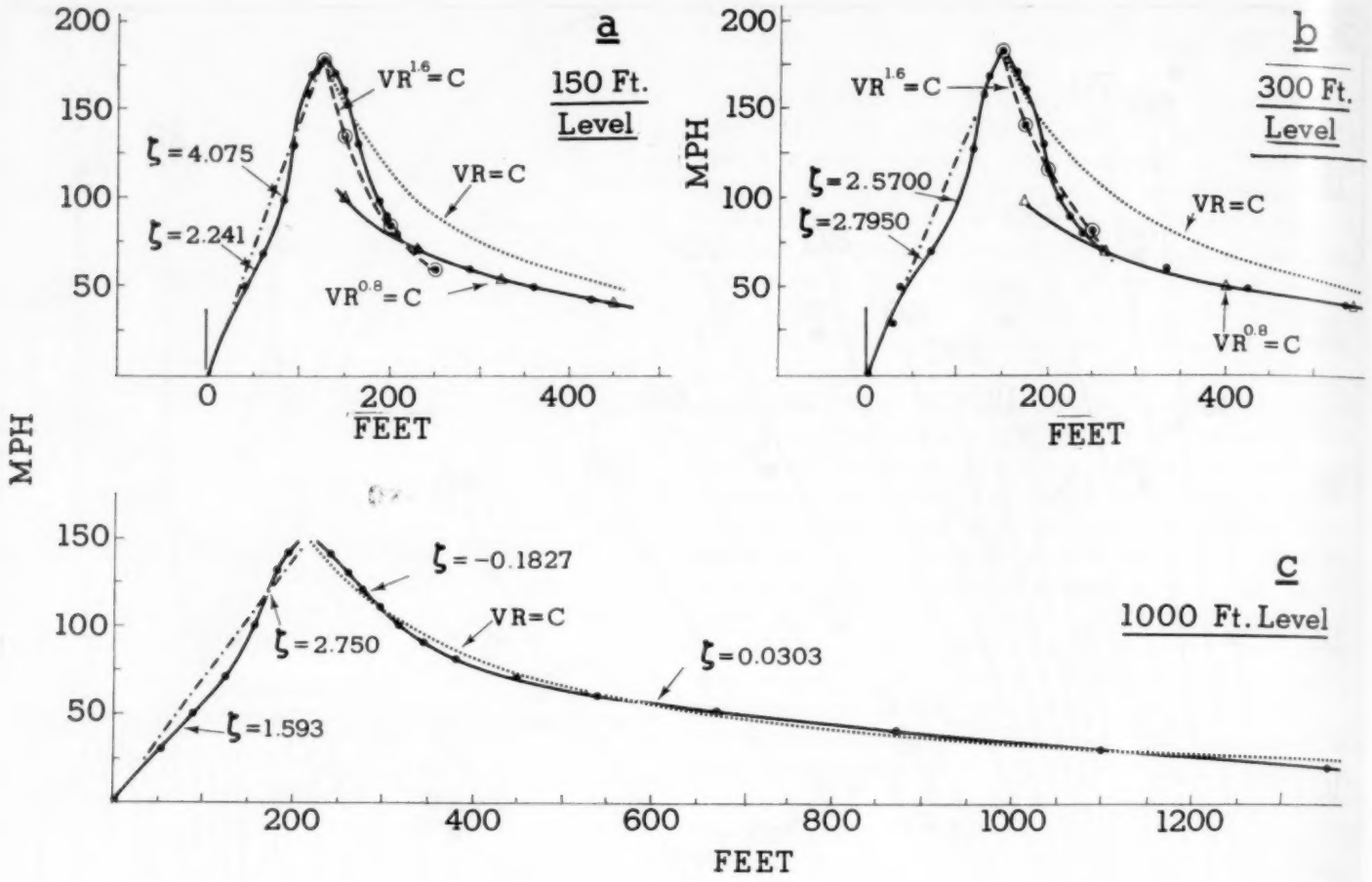


FIGURE 3.—Variation of tangential speed with radius for elevations of 150, 300, and 1000 ft. as taken from the analysis of figure 2. Data taken from analyzed isotachs.

rather sudden packing of the isotachs inside of the 70-m.p.h. isotach; this item will be discussed in detail later. The high-speed points at the 200- and 270-ft. levels (near the center in the enlarged inset) where low speeds should be expected, might be due to errors in determining the radii of these particles. The low-speed data points in the high-speed band near the 300-ft. level may have been derived at a time when the tornado speed was temporarily slackened at those locations, or again there could have been errors in determining the radii. The two data points at about a radius of 150 ft. and at 1475 ft. and 1940 ft. in elevation are too high in speed for the arrangement of the isotachs in figure 2. However, they were taken late in the lifetime of the tornado when the funnel became quite tall and narrow. Earlier no measurements had been possible at those locations since the funnel cloud occupied that region.

The inset of figure 2, which doubles the size of that portion of the figure enclosed by the dotted lines, shows the size of dwellings and trees to scale relative to the size of the isotach speed distribution. One-half of a city block extends from the left edge of the drawing to the 220-ft. mark. The rapid increase of speed upward into the band of maximum speed in the lowest 100 ft. above the ground coupled with the second-power increase of wind force with speed, shows how tree tops could be broken off while houses would be relatively undisturbed. The decrease of speed horizontally outward from the maximum speed band is rapid, indicating how a narrow zone of damage cut-off could occur. By way of comparison the minimum speeds required to cause yielding of certain building structures in and near the path of the Dallas tornado were reported by Bigler and Segner [1] to range from 55 to 220 m.p.h. These structures ranged in height up to about 20 ft. above the ground for the most part.

From the isotach analysis of the tangential speeds as presented in figure 2, plots of speed versus radius were made for elevations of 150, 300, and 1000 ft. above the ground and are presented in figure 3. These levels were selected because they were located where the better data distributions existed. For the 150- and 300-ft. levels (figs. 3a and 3b) the observed speed curves (solid lines with dots) show a steeply-sloped inner portion exterior to the point of maximum speed out to about the 250-ft. radius and a shallowly-sloped outer portion in the region exterior to about the 250-ft. radius. A definite break in the slopes between the inner and outer portions is evident. A comparison of these curves with the $VR$=Constant curves

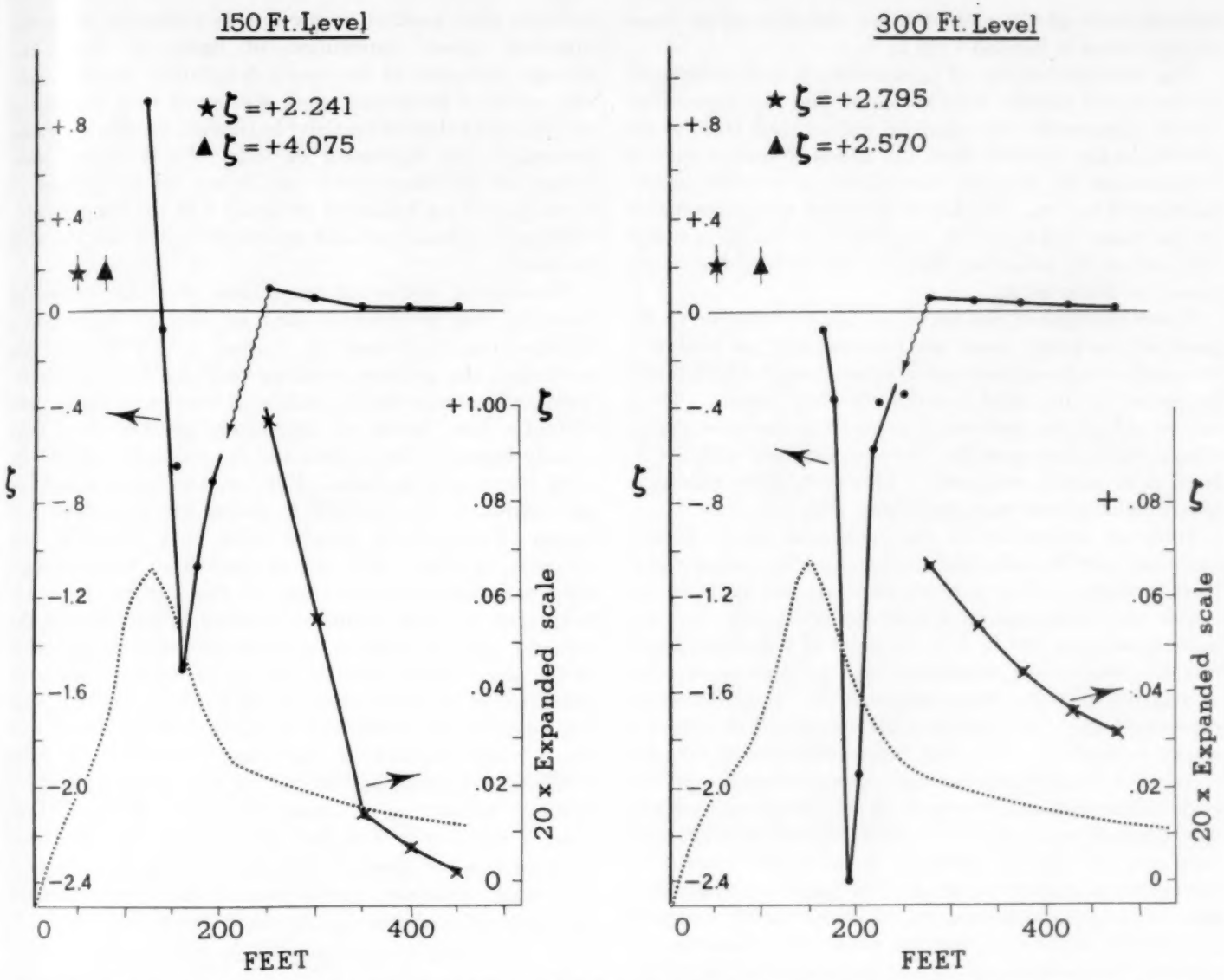


FIGURE 4.—Variation of vorticity with radius at the 150- and 300-ft. levels using tangential speeds from figure 3. A 20-times expanded scale is provided for the portion exterior to about 225 ft. in radius.

(dotted lines) on these graphs shows considerable deviation, indicating that the observed speed distributions were not irrotational. However, curves with $VR^{0.8}$=Constant were fitted to the shallowly sloped outer portions; the fit is very good, as shown by the open triangles. For interest these curves were continued inward nearly to the radius of observed maximum speed. No attempt was made to fit the steep, inflected inner curves with a simple mathematical curve. However, the slope was approximately averaged by the curve $VR^{1.6}$=Constant (dashed curve with circled dots).

The observed curves show that the air flow in the vortex exterior to the break in the curves (about 250-ft. radius) was rotational in the positive sense (cyclonic) and in the negative sense (anticyclonic) interior to the break point. It is presumed that surface and internal frictional effects caused the slow rate of increase in speed inward between radii of 550 and 250 ft. and prevented the conservation of angular momentum. Inward from the radius of maximum speed the deviation of the curves to speeds less than that required for solid rotation may reflect the effects of friction at the ground. However, the deviation is not great.

A rather accurate distribution of observed (derived) tangential speeds at 1000 ft. above the ground and out to a radius of 1360 ft. was provided by the tracking of cloud tags near that elevation at small intervals of radius. This distribution is shown in figure 3c as the solid curves with dots. The slope of this speed distribution curve is considerably more shallow than the slopes of the curves for the lower levels. Surprisingly enough, the portion of this curve exterior to the radius of maximum speed follows quite closely the theoretical $VR$=Constant curve (dotted line) as shown on the graph. The observed curve drops a little below the theoretical curve between radii of 290 and 575 ft., comes slightly above the theoretical curve

between radii of 575 and 1100 ft., and then again drops slightly below it beyond 1100 ft.

The near-conformity of the observed and theoretical curves at the 1000-ft. level indicates that the irrotational vortex apparently can exist in nature and that where conditions are removed from the effects of surface friction conservation of angular momentum is possible in the convergent vortex. The lag of observed speed (compared to the theoretical speed) in the region of 350 ft. in radius may reflect the retarding effect at this level of the slower speeds at lower levels.

Those portions of the curves of figure 3 interior to the point of maximum speed are inflected and, as analyzed, do not show a linear decrease of speed inward which would be necessary for solid rotation in that region. These curves reflect the manner of analysis in the core region where direct interpolation between higher- and lower-level data points was made. However, these nonlinear speed distributions may have been real.

Since an inspection of the tangential speed curves, described above, indicated that the portion of the low-level tornado air flow exterior to about 250 ft. from the center was rotational in a cyclonic sense and that the portion between 250 ft. and the point of maximum speed was anticyclonically rotational, the vertical component of relative vorticity was computed for these curves at several points. The variation of vorticity with radius is shown in figure 4. The solid curves with dots in the two sections of the illustration show the variation of vorticity with radius relative to the scale on the left of each section. The absolute value of positive vorticity was much smaller than that of negative vorticity in the region exterior to the radius of maximum speed. The large values of negative vorticity were related to the steepness of the speed distribution curve. So that the reader may compare the vorticity distribution against the distribution of tangential speed, the speed distribution curves from figure 3 are shown as dotted curves in figure 4. To show the radial variation of positive vorticity to better advantage, the vorticity values were plotted at the right-hand side of the graphs on a scale 20 times larger than the left-hand scale. The steeply rising curves (through crossed dots) to the right in each panel of figure 4 are fitted to the expanded scale. The vorticity distribution curves are discontinuous at the same locations that the speed distribution curves are discontinuous.

Since the observed and theoretical tangential speed curves coincided so closely at the 1000-ft. level no computations of vorticity distribution with radius were made for that level. However, two point determinations were made and were plotted on the curve of figure 3c. One at the 300-ft. radius was $-1827\times10^{-4}$sec.$^{-1}$ in the region where the observed curve was steeper than the theoretical curve. Another at the 600-ft. radius was $+303\times10^{-4}$ sec.$^{-1}$ in the region where the observed curve was less steep than the theoretical (nonrotational) curve. Those portions of the flow inside the radius of maximum speed indicate high positive vorticities as computed with the observed speed distribution of figure 3. Since the average steepness of the speed distribution curves inside the radius of maximum speed steepened with decreasing altitude the values of vorticity in that region also increased generally with decreasing altitude. Point values computed for the three levels are shown on the curves of figure 3, and are indicated on figure 4 at the proper radii. Maximum values exceeded $4000\times10^{-3}$sec.$^{-1}$ for the 150-ft. level.

Considering orders of magnitude of these values of vorticity, one is reminded that an average figure for a middle-latitude cyclone is around $2\times10^{-4}$sec.$^{-1}$. Accordingly, the greatest positive vorticity for the 150-ft. level and exterior to the radius of maximum speed was virtually four orders of magnitude greater than that usually found in the cyclone and the value for the 300-ft. level was nearly as high. Further, the value found for the 1000-ft. level at the 600-ft. radius was more than two orders of magnitude greater than that found in the synoptic cyclone. This means that there was considerable horizontal concentration of the vertical vorticity field, that is, much vertical stretching in and around the tornado, and in addition, more horizontal concentration in the lower levels than in the upper levels. Using the principle of conservation of potential vorticity and neglecting compressibility it is found that convergence of air, having vorticity of the order of $10^{-4}$sec.$^{-1}$, from 5 miles away would provide the greatest value of positive vorticity found here at about the 250-ft. radius. However, if vorticity in a region favorable for the formation of tornadoes was greater than $10^{-4}$sec.$^{-1}$ the advection to the center would not have to come from so far to provide the large value of vorticity found in this tornado.

## 3. VERTICAL SPEEDS

While the tangential wind speeds were being obtained by means of the cloud tags and the temporarily suspended solid debris particles (as in fig. 1), vertical components of motion were observed and measured in the cloud tags and it was realized that vertical motion of the air was required to suspend the solid objects. When cloud tags were tracked, the vertical speed of the tag was taken as the upward air current speed at the radius where it was found. When pieces of debris were tracked, some allowances were necessary regarding their terminal falling speed in still air. Fortunately, during the period that was investigated, the tornado had picked up, possibly from a lumber yard, a large number of thin sheets of material, all of which were about $4\times8$ ft. in size. These objects were used for most of the low-level speed measurements. The movie showed that they were tumbling, which would give them a rather uniform falling rate. Hence, the falling rates of about a dozen of these pieces were measured when they appeared to be far enough from the tornado's influence to reach a nearly true terminal falling speed relative to a stationary atmosphere.

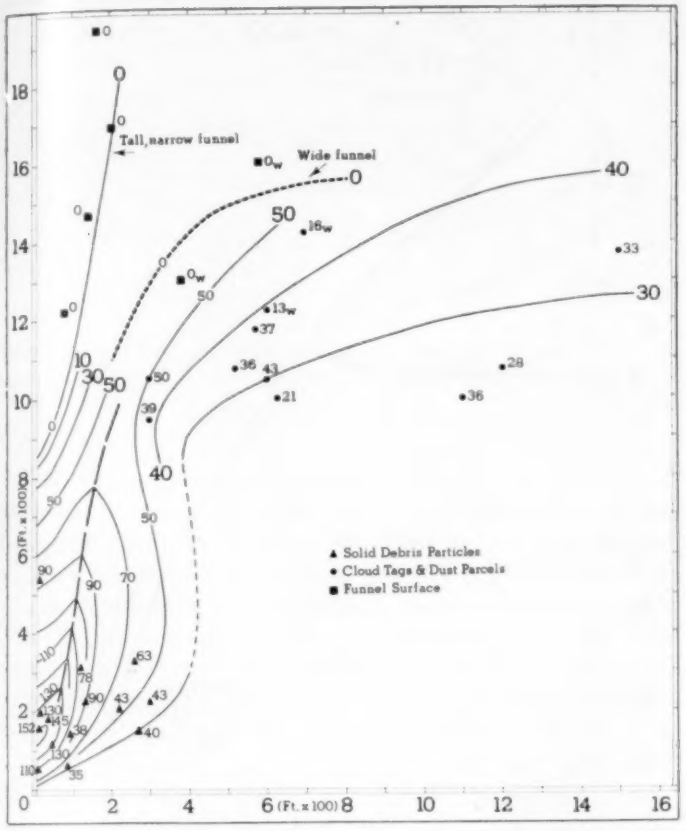


FIGURE 5.—Distribution of derived upward speed from the center of the tornado to about 1500 ft. in radius and from the ground to about 1700 ft. in elevation.

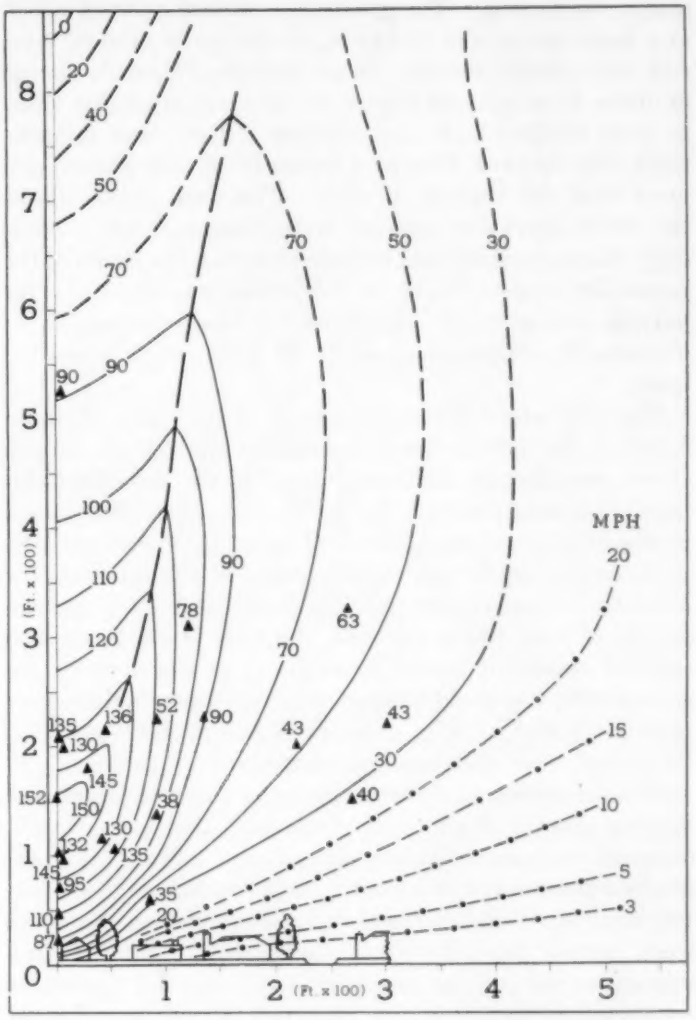


FIGURE 6.—Detailed version of distribution of upward speeds. Only the lower 900 ft. and the inner 500 ft. are shown.

These speeds averaged 43 m.p.h., with only a little scatter. Accordingly, when any of these 4×8 ft. pieces were tracked for vertical speed, a correction of 43 m.p.h. was added algebraically to whatever vertical speed the particles had relative to the ground. The radius of the path was already available for each particle from the tangential component measurements. Since there are fewer data points for vertical speed than tangential speed, there is less confidence in the distribution of the vertical speed isotachs than for the horizontal speed isotachs in some portions of the tornado.

Figures 5 and 6 show the distribution of the upward speed data points around the tornado and the isotachs fitted to them. The center of the tornado is along the vertical scale at zero radius. Figure 5 shows the overall picture and figure 6 the lower 800 ft. in greater detail. The fit of the isotachs in figure 5 shows a relatively small low-level core of high-speed upward air flow at about the 135-ft. elevation. The maximum derived upward speed was 152 m.p.h. Above the high-speed jet at an estimated elevation of 850 ft., the upward speed became zero and from this point the zero isotach sloped upward with increasing radius in a manner, at any one time, apparently depending upon the shape and size of the funnel. Late in the lifetime of the tornado the zero-speed envelope was in a narrowly tapered shape somewhat as outlined by the zero isotach in the upper left of the diagram and labeled as "tall, narrow funnel." The condensation funnel at the later stage actually extended to the ground but it was impossible to determine the level at which zero vertical speed began in the core. At an intermediate time stage the zero-speed envelope lay approximately along the dashed curve in a form to agree with the zero upward speed data points marked with a subscript "w" and also agreeing with the shape of the funnel at that time. The zero speeds were found by tracking cloud fragments on the funnel surface. The "w" indicates that these data points were taken when the top of the funnel was wide compared to those taken at a later stage. The two upward-speed data points subscripted with "w", and located in the region of about 1300 ft. in elevation and 700 ft. in radius, have values much lower than surrounding data points. They were derived by tracking cloud parcels a relatively short distance from the condensation envelope at a time when the envelope was relatively wide.

In the region above the 900-ft. level and outside the 400-ft. radius the isotachs turn outward and become

nearly horizontal. The greatest measured upward speed at a large radius was 33 m.p.h. at about the 1400-ft. level and the 1500-ft. radius. Since measured upward speeds of about 55 m.p.h. are known in thunderstorms this value is quite realistic. At some larger radius these isotachs must turn upward, then at a higher level turn inward and meet over the tornado system. The data points above the 900-ft. level were derived from cloud tags and accordingly these speeds should be correct within the limits of the measuring system, since no correction was necessary for particle falling speed. Additional evidence in support of a region of no upward speed in the core will be presented later.

Figure 6, which is an enlargement of the region of figure 5 below the 900-ft. level and inside the 500-ft. radius, shows considerable additional detail of the isotachs (solid lines) and data points. At the bottom of the illustration is shown to scale the ½ block of trees and dwellings (the same as for fig. 2) and their relation to the upward-flow isotachs. Observe how tree tops could extend into upward speeds of over 100 m.p.h. and the tops of dwellings into upward speeds of nearly 90 m.p.h. As the isotachs are shown here, this could happen only very close to the center of activity and so only a narrow region of damage would be caused from this upward component. Movies of the Dallas tornado actually show pieces of shattered dwellings moving upward in and around the core, then being tossed outward at some relatively low height. None of these pieces was observed to ascend initially outside of the dense, but small-sized, debris cloud; it is assumed then that they were carried upward within the narrow region of high upward speed. Upon reaching lower upward speeds at some higher elevation (an elevation where an outward component must exist), the pieces were ejected and then dropped since upward speed was insufficient to support them.

The data points near the center of the tornado and below 300 ft. in height show how the high speed upward current split into a cone-like form around the core (an arrangement that was mentioned earlier) such that above about 150 ft. in height the upward speed in the core was slower than the air immediately outside it. It was almost as if the air flow split around a pointed cone somewhat as around a sharp airplane nose. In the lower portion of figure 6 are some theoretical isotachs of vertical speed indicated by the dot-dash lines. They were included to show how nicely they fit with the observed isotachs. The procedure for generating them will be described later.

As will be seen in figure 6, some of the data points do not fit the analysis; examples are the ones at the 225-ft. level, 90-ft. radius (52 m.p.h.) and the 135-ft. level, 90-ft. radius (38 m.p.h.). The policy of showing all reasonable data points obtained (as was used for fig. 2) is retained here. The only exceptions were some points located below the 30-m.p.h. observed isotach that were much too high for both the observed and theoretical speeds.

In order to test the observed vertical speed distribution

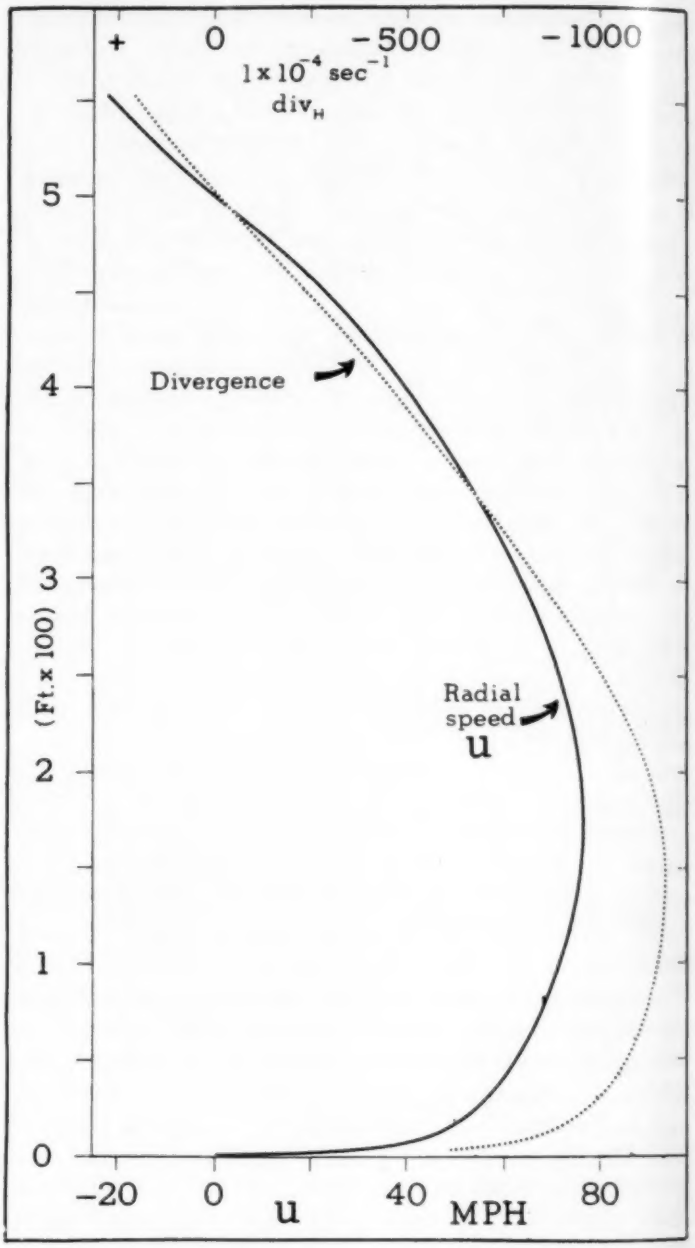


FIGURE 7.—Distribution of assumed radial speed, $U$, with elevation at the 500-ft. radius (solid line, using the scale at the bottom) and the distribution of horizontal divergence with height at the 500-ft. radius (dotted line using the scale at the top).

of figure 6 for consistency in the region exterior to the location of maximum upward speed and below 600 ft. in elevation, a theoretical vertical speed distribution was constructed. It was based on the principle of continuity, the assumption of incompressibility, and use of a convergent radial speed ($U$) distribution of the form $U \propto 1/R^n$, where $0 < n < 1$; inward flow is designated as positive in the following analysis. The assumed distribution of $U$ with height at the 500-ft. radius was adapted from a graph of low-level wind-speed distribution with height, published by the Weather Bureau [6]. It was modified

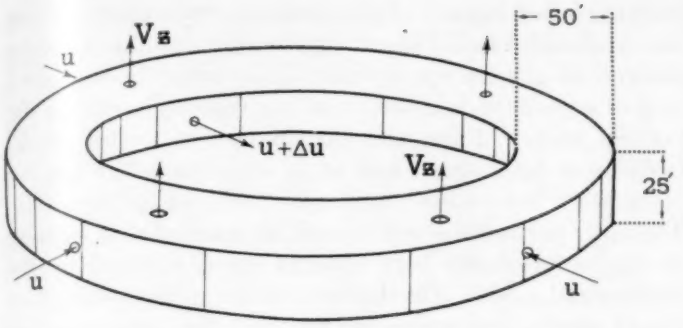


FIGURE 8.—Volume element used in computing theoretical upward speed distribution from the assumed radial speed distribution.

so that $U$ reached a maximum at the 175-ft. level, decreased to zero at the 500-ft. level, and then reversed to outward flow above 500 ft. This distribution with height is shown by the solid curve in figure 7. The horizontal radial-component speed at 6.25 ft. above the ground and at the 500-ft. radius was taken as 40 m.p.h. and directed toward the center. The values of $n$ used were 0.4 from the ground to 100 ft. in elevation, 0.5 from 100 to 200 ft. in elevation, and 0.6 for elevations above 200 ft., so as to be consistent at least qualitatively with decrease of frictional drag at increasing distances above the ground. Vertical speeds were computed from the time rate of excess volume accumulating in rings of unit volume around the tornado which were 50 ft. wide and 25 ft. deep, one of which is shown in figure 8. Above 212 ft. in elevation, the rings were 50 ft. deep. The vertical speed coming out of each ring was accumulated from the ground upward such that a distribution of vertical speed was obtained from the 500-ft. radius inward and from the ground to a little over 600 ft. in elevation.

The resulting distribution of computed upward speeds with height and radius is shown by the solid curves of figure 9. Not all the computed data points are shown but the isotachs were drawn with all of them in consideration. For comparison with the isotachs of theoretical upward speeds, the observed speeds from figure 5 are reproduced as dashed lines in figure 9. Considerable agreement is shown by the near fit on the 30-, 50-, and 70-m.p.h. isotach lines. But the 90-m.p.h. observed isotach is considerably nearer the center of the tornado than is the theoretical line. Nevertheless, where agreement in speed is poor the trend of the theoretical and observed lines is nearly the same. Increasing the radial speed $U$ inward from about the 250-ft. radius only, and keeping the outer portions as described above, brought the 90-m.p.h. theoretical isotach into near coincidence with the 90-m.p.h. observed isotach and at the same time kept the 30-m.p.h. isotachs in close proximity. However, the 70- and 50-m.p.h. theoretical isotachs moved inward away from their positions of near coincidence in figure 9, and the computed isotachs lost their smoothly curved characteristics. Undoubtedly distributions of $U$ with

554818—60——2

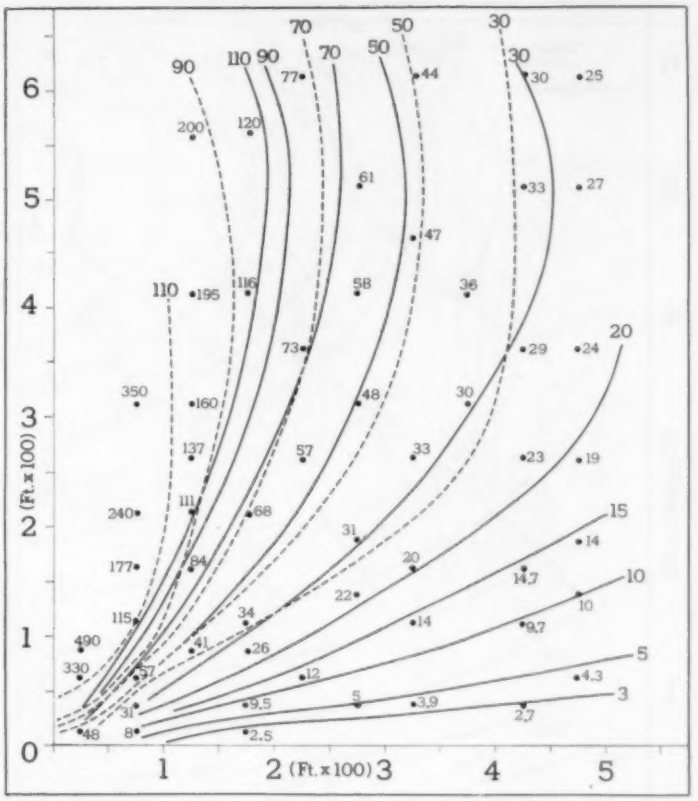


FIGURE 9.—Distribution of theoretical upward speed (solid lines) computed from the assumed radial speed distribution of figure 7 (solid curve). Dotted lines are isotachs of observed upward speed.

radius could be devised that would give even better approximations than those shown here, but the effort to find them is time consuming. Here at least, it has been shown that a good approximation to a portion of the observed distribution is possible. Perhaps if the volume of air specified by the method did truly ascend in the middle of the tornado the observed upward speed distribution near the center would more nearly coincide with the theoretical distribution. Very likely the separation of the vertical high speed jet into a shell around the less speedy tornado core at high levels accounts for the observed increase being less rapid than the theoretical increase of upward speed inward from about the 200-ft. radius.

For the purpose of comparison of convergence in other observed tornadoes and thunderstorms, the convergence in the specified horizontal wind system of the Dallas tornado was computed. The computation was made at the 500-ft. radius and in steps from 6.25 ft. to 550 ft. above the ground. The same radial speed distribution with height was applied that was used in constructing the theoretical vertical speed distribution (see fig. 7). The convergence values range from $700\times10^{-4}$sec.$^{-1}$ at 6.25 ft. above the ground to a maximum of $1175\times10^{-4}$ sec.$^{-1}$ at about 150 feet above the ground. The results are displayed on figure 7 as the dotted curve with the scale

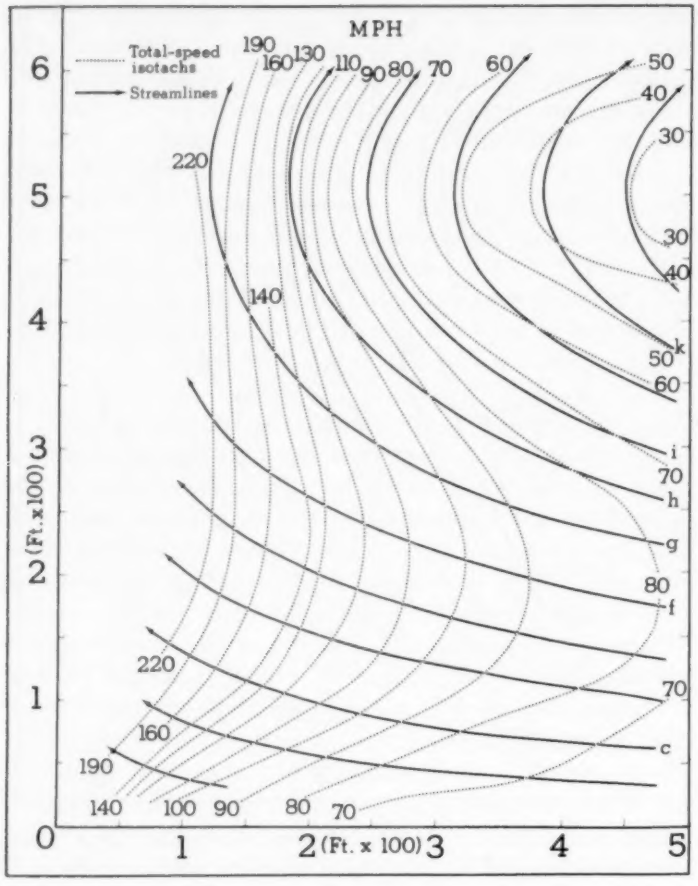


FIGURE 10.—Computed trajectory and isotach pattern in the vertical plane through the lower portion of the tornado.

at the top of the graph applying. Convergence went to zero at the 500-ft. elevation as required by the distribution of $U$ in figure 7. The maximum value quoted above is approximately four times greater than the convergence found by Fujita [4] in the Fargo, N. Dak., tornado of June 20, 1957, at a radius of about 3000 ft. and an elevation of 3000 ft. Convergence in the Dallas tornado was also computed from derived radial wind components obtained from movement of industrial smoke plumes near the tornado (Hoecker [7]) for a radius of 0.75 mile and elevation of about 600 ft. These values were around $350\times10^{-5}$ sec.$^{-1}$, about 1/35 of the maximum value computed above from synthesized values of radial speed (see fig. 7) at the 500-ft. radius. Additional comparison comes from data obtained in the Thunderstorm Project [2], where it was found that precipitating Florida thunderstorms provided convergence between $250\times10^{-4}$ sec.$^{-1}$ and $850\times10^{-4}$ sec.$^{-1}$, the latter between 16,000 and 20,000 ft. in elevation. The larger figure for the thunderstorms was about two-thirds of that found for the Dallas tornado at the 150-ft. level and 500-ft. radius, using the synthesized inflow data.

Inasmuch as the theoretical distribution greatly resembled the observed distribution of upward speeds, at least in certain regions of the tornado, it was assumed that the synthesized radial speed distribution and the resultant theoretical upward speed distribution could be combined to give a realistic distribution of the velocity vector in the vertical plane. From this distribution of vector winds, isotachs of total speed and some trajectories* in the $r$–$z$ plane were determined and are displayed as figure 10. The inner portion was left vacant, as it was earlier, because of the unreasonably high upward speed required by the synthesized model. On the basis of the initial assumption stated above, it is presumed that the trajectory analysis of figure 10 closely resembles the actual trajectories that existed at times in the tornado flow.

As shown in figure 10, the trajectories have a definite upward component throughout the region represented; this is required for the convergent regime of the radial component of wind. And, as required by the distribution of $U$ with height (shown as the solid line of fig. 7) the trajectories show a reversal to outward flow above the 500-ft. level. Note that the curvature of the trajectories at the 500-ft. level is greater at larger distances from the tornado. Trajectories entering the illustration from the right below 300 ft. in height cross over to regions of greater speed while those entering above 300 ft. cross over to regions of lower speed ending at the 500-ft. level. Above 500 ft. they enter regions of increasing speed. There is the suggestion of a closed circular movement of air in the shape of a ring vortex around the tornado, having a horizontal axis at the 500-ft. level and a little outside the 500-ft. radius. This suggestion is augmented by the shape and movement of the outer and upper edge of the more dense debris cloud where in both still pictures and movies an outward and downward curling motion takes place. This curling action is typified in the upper right-hand portion of the schematic debris cloud shown in figure 1.

Mass divergence in the steady-state system of figure 10 is required to be zero, but attempts to prove this encounter difficulties such as determining the distribution of density in the system. However, on an assumption of incompressibility, zero velocity divergence was imposed on the system by the manner of determining the upward speed distribution from the elemental volumes of figure 8.

## 4. THE THREE-DIMENSIONAL FLOW

The vector flow distribution in three dimensions below the 600-ft. level and inward from the 500-ft. radius was determined using the vertical plane trajectories of figure 10 and horizontal streamlines. The horizontal streamlines at given levels were obtained by vector addition of the computed radial component regime, described earlier, and the observed tangential wind speed. Again the assumption was used that since the computed upward speed distribution closely resembled the observed upward speed distribution (at least outside the central core region) the synthesized radial speed distribution closely resembled the

*Because of the implicit steady-state assumption, streamlines and trajectories coincide.

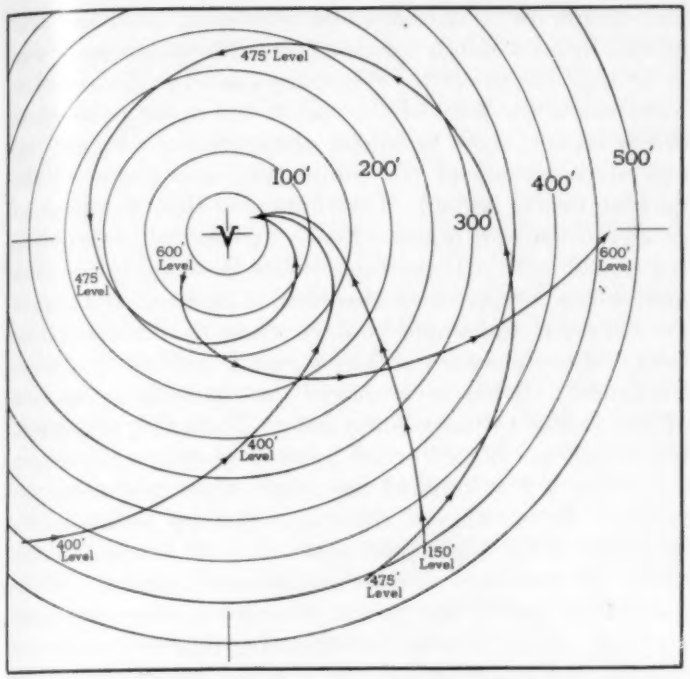


FIGURE 11.—Horizontal streamline patterns for several levels of the tornado in the lower 600 ft.

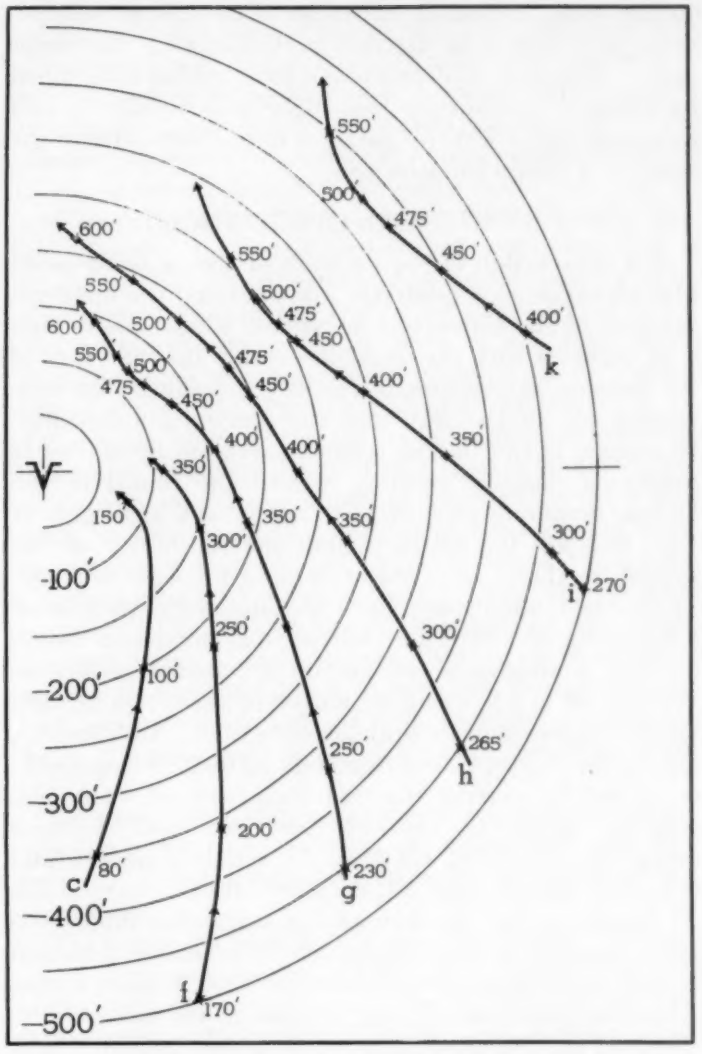


FIGURE 12.—Horizontal projections of the three-dimensional trajectories of some air parcels which also follow the trajectories of the vertical projection in figure 10. Key letters identify identical trajectories in figures 10 and 12.

actual, but unmeasurable, radial wind speed distribution. Horizontal streamline patterns were computed for 50-ft. vertical intervals from 50 ft. in elevation to 600 ft. in elevation with an additional level at 475 ft.; some of the significantly different patterns are shown in figure 11. In order to emphasize the differences in streamline curvature with elevation the end points of the several streamlines have been made to coincide. Note the predominantly radial component for the 150-ft. level and the increased tangential component at the higher levels. The horizontal streamlines for the 500-ft. level would, of course, be concentric circles. At the 600-ft. level the streamlines are divergent as indicated in the figure.

The horizontal projection of some of the three-dimensional trajectories are shown in figure 12. Along each trajectory are shown the starting elevation and the points at which the trajectory passed each 50-ft. level. (The crossed dots are not data points.) The key letters at the start of each trajectory refer to identically keyed trajectories in the $r$–$z$ plane of figure 10. These trajectories were constructed by following the horizontal streamline pattern in each 50-ft. vertical interval bracketing a standard level (i.e., 75 to 125 ft. for the 100-ft. level, etc.). Segments for each height interval were connected resulting in the trajectories of figure 12. The radius of each segment was controlled by the corresponding trajectory in figure 10.

One of the interesting features of these trajectories is the generally small curvature in the horizontal plane. Only trajectories "c" and "f" curve sharply and then only inside the 150-ft. radius. The others seem merely to cut across an edge of the tornado.* Trajectory "i" through part of its track is convex to the tornado and trajectory "k" is entirely convex. These trajectories show that in the region below the 500-ft. level and at the 500-ft. radius, the higher the entry elevation for the air parcel the less closely it approached the center of the tornado. Unfortunately, the radial inflow assumption did not generate the observed vertical components in the center of the tornado and so the trajectories in that region were not computed.

It is thought that the three-dimensional trajectories are quite representative since there was some similarity between the trajectories of figure 12 and the paths of the particles flying around the tornado, as seen in one of the Dallas tornado movies. In the movie the particles are, in many cases, thrown out ahead of the tornado in the direction of its motion after having been lifted into the circulation. As the particles were brought inward and upward, they entered a region of decreasing inward com-

*Illustrating the domination of tangential speeds over radial speeds except in the lowest levels.

ponent wind, eventually encountered an outward component, and were then ejected, particularly at the larger radii. This type of debris movement has been described by tornado eyewitnesses (see Bigler and Segner [1], and Dinwiddie [3]). Centrifugal force most likely aided in the ejection of debris particles also.

## 5. NONTYPICAL OBSERVATIONS

The observation of the decrease of core upward speed with elevation at a relatively low level and the apparent splitting of the high-speed jet around a less speedy core is at variance with the usual conception that the core of the tornado participates in the sink mechanism for converging air all the way into the parent thunderstorm. In support of this finding is the observation by movies of roughness elements rotating around the funnel of the Dallas tornado at radii of 75 to 200 ft. and at heights of 1500 to 1900 ft., where, within the sensitivity of the scaling method, no vertical movement was detected. There could, admittedly, have been upward movement of a low order of magnitude, but whereas horizontal movement of a roughness element on the funnel surface as small as 40 m.p.h. could be measured easily, no upward movement was detectable at the same time. Additionally, among the movies of four tornadoes on file, it is impossible to detect for certain, upward movement of roughness elements along the condensation envelope of these tornadoes. Much of the time the trunk is smooth and not even ripples can be detected along the surface. Of course, in the tip region of a suspended funnel the hazy character of the condensation funnel makes detection of movement almost impossible even though rapid fluctuations in optical density are evident in the movies.

One of the Dallas tornado movies shows upward movement of optical density discontinuities in the hazy, lower portion of the suspended tip region when it was several hundred feet above the ground and quite narrow. The upward jet was feeding into the condensation trunk tip region at this time and possibly was effective in hindering condensation there. Upward speed did not appear to increase with elevation along the flow path. An observation at very close range by Dinwiddie [3] of a waterspout-turned-tornado agrees qualitatively with the observed upward speed distribution indicated by figure 6 in the region below the 300-ft. level and inward from the 100-ft. radius. Dinwiddie describes objects being carried aloft to a certain level, being momentarily suspended, then ejected outward and downward. He concluded that there was a high-speed upward jet close to the ground whose upward speed eventually decreased with height.

Many still photographs of tornadoes and their attendant debris clouds indicate that the major sink region is exterior to the condensation funnel. For example, when the condensation trunk tip is at or near the ground the width of the rotating debris cloud is greater than when the trunk is suspended aloft. The writer has never seen a photograph of a debris cloud extending outward and upward from *within* a tornado trunk while the trunk was at or near the ground. When the funnel extends downward below the level of the top of the dense particulate debris region, there is almost always a clear region immediately outside of the funnel wall and inside of the darkest debris region. This indicates that a region of greater density of debris extends upward while avoiding the funnel itself. If the funnel were involved in the sink mechanism for the cases observed, it seems that some of the finer material would be drawn into the funnel and so tend to de-emphasize the clear region immediately around the funnel. It has been noticed that, at least in the case of the Dallas tornado, more debris (including chunks of buildings) was being carried upward when the funnel tip was lifted a few hundred feet than when it was on the ground. It is believed that when the tip is lifted, the elevation of the high-speed upward jet is relatively high above the ground or at least is elongated upward. When the funnel touches the ground, it appears that converging air turns upward through a larger ring-shaped area so the maximum upward speed for a given sink strength is reduced and no central high speed core exists. However, upward speed is still sufficient to lift some lighter debris. Observational evidence in support of this idea is contained in a sequence of photographs of another tornado on file which showed the ground-based debris cloud increasing in diameter as the suspended funnel widened and lowered toward the ground. No debris was seen to rise in the region beneath the cut-off tip of the condensation funnel but all of it ascended exterior to the tapered cylindrical funnel which widened upward. In the pictures and movies of the Dallas tornado no large clouds of dust or spray, or chunks of structures were observed ascending along the trunk when the trunk was touching the ground. Had any large chunks been carried upward inside the funnel, surely a few would have been thrown outward through the funnel wall by centrifugal force much as they were observed to do when the funnel tip was retracted.

As a means of explaining a decrease of upward speed with height above the low-level high-speed core, the following idea is suggested: If the bent-down isobaric surfaces in this tornado were spaced, in the vertical, farther apart at the center than at larger radii, then there would be less upward accelerating force in the center. For example, if at some location spacing allowed an upward pressure gradient force that just balanced the pull of gravity, there would be no net upward force (excepting frictional force) on the air at that location and so a decelerating tendency would take place.

Some question undoubtedly arises as to the mechanism that removes the volume of air that continuously flows toward the tornado center in the lower levels. It is suggested that the flow in the tornado must take on an outward component above the level of maximum upward speed. This would allow the narrow, low-level upward jet to spread out over a larger area at higher elevations so

that a lower-speed, larger-area updraft around the tornado could easily remove upward the low-level convergent volume. The flattening out of the observed updraft isotachs around the tornado at higher elevations and larger radii shows some evidence for this suggested mechanism.

A rough volumetric test was performed to compare the flow rate through the 1200-ft. level out to 1600 ft. of radius with that through a surface at the level of the maximum-speed jet (150 ft.) out to 300 ft. of radius using upward speeds from figures 5 and 6. A uniform upward speed of 30 m.p.h. was used for the upper surface, 120 m.p.h. for the inner 100 ft. of radius, and 70 m.p.h. for the outer 200 ft. of radius for the lower level. Incompressibility was assumed. The flow rate through the upper surface computed to more than one order of magnitude greater than that through the lower surface. The upward speed used for the upper surface is a minimum and therefore the sink at 1200 ft. as computed would take care of a source strength more than ten times as great as provided by the lower surface.

It is also possible that some of the low-level air recirculates as is suggested by the turning outward and downward of the outer rim of the low-level dense debris cloud. This would require less volume to be removed at higher levels.

The reversal of radial inflow to one of outflow at some elevation (for this case, estimated to be at 500 ft. above the ground) is also at variance with generally accepted ideas of tornado flow mechanics. However, general spreading of the lighter debris particles with height up to the tornado-associated cloud base is indicated in many tornado photographs and is demonstrated in movies. If general indrafts into the trunk existed around this region there should be a concentration of the lighter material around the upper portion of the tornado and a tapering inward with height of the lightly shaded (that portion offering low optical density) and higher-level debris cloud. Such has not been found in the Dallas tornado photographs. However, in some tornadoes optically dense debris has been photographed ascending along the tornado trunk in a cylindrical shape as contrasted to the tapered outward and upward shape that so characterized the dense debris cloud of the Dallas tornado. In those cases the trunk was usually lowered to near the ground and was quite wide, and it is thought that such instances represent a particularly energetic stage of the tornado. The effect seen may be in the nature of a transient surge of air inward at low level and upward along the trunk which carries heavier particulate debris to higher elevations. Evidently the air flow pattern of the tornado is complex and changes from one tornado to another and may change from time to time in any one tornado.

## 6. CONCLUDING REMARKS

For the first time a distribution of observed tangential and upward air speed in a tornado has been obtained. This was made possible by the use of tornado movies of high quality and the utilization of the methods of photogrammetry and perspective. Further, a convergent radial speed distribution was synthesized that produced an upward speed distribution quantitatively close to the observed upward wind speed distribution in the lower 600 ft. of the tornado. The three components (i.e., synthesized radial distribution, generated upward distribution, and observed tangential distribution) were combined to determine the three-dimensional air parcel trajectories for the lower portion of the Dallas tornado. These trajectories resemble the paths of some of the solid debris particles which were thrown out ahead of the right-hand side of the tornado after being lifted in the core.

From the analysis of the radial distribution of the tangential speed, vorticity distribution was determined at three levels. Large values of negative vorticity were found at small radii (but exterior to the radius of maximum tangential speed) and at low levels, and the $VR$=Constant relationship did not hold. At the 1000-ft. level, however, the $VR$=Constant distribution was nearly attained. Immediately outside of the region of maximum speed and at 150 and 300 ft. in elevation, the speed change with radius approached a $VR^{1.6}$=Constant relationship, while at greater radii a $VR^{0.8}$=Constant relationship was evident.

Extremely high tangential speeds were not found and 170 m.p.h. was the maximum, although there may have been higher speeds where tracers were not tracked or were absent.

The upward speed distribution was found to have a jet of maximum speed at about 135 ft. above the ground at the core; it decreased above that to zero near the 1000-ft. elevation. At a radius of 300 ft. the maximum upward speed in the lower levels was at the 400-ft. elevation, however. An envelope of zero upward speed was found above the 1000-ft. level which appeared to coincide with the condensation envelope.

Evidence was found in the distribution and movement of small particulate debris around the tornado to indicate that the upward flow took on an outward component above the region of maximum upward speed.

Some nontypical observations showed that no upward air flow was detectable on the surface of the funnel at levels above about 1000 ft.; only tangential components were detected. A suggestion was made that the condensation funnel, with the exception of the lowest portion of the suspended tip section, does not participate in the upward sink mechanism. Evidence in support of this idea is contained in movies and still photographs showing more debris being carried upward beneath the suspended funnel than when the funnel was on the ground and in sequential photographs showing a widening of the debris cloud into a ring shape at the ground as the funnel lowered and widened. The diameter of the debris cloud at ground level equaled or exceeded the diameter of the lower end of the condensation funnel.

The implication is that had the region in and beneath the lowering and widening funnel been involved in the sink, the debris would have converged to a small region beneath the lowering funnel rather than being turned upward at some larger diameter. The visible funnel does not control the sink distribution but only exists in the region of little or no upward air movement. Certainly air ascends in the vortex core beneath the suspended funnel tip and ascends around the exterior of the funnel whether it is suspended aloft or is on the ground.

Hence the air speed in the unmeasurable tornado has finally been measured and the speed distribution compared with theoretical distributions. To what extent other tornadoes differ from the Dallas tornado is not known but the disposition of the condensation funnel and the attendant debris cloud in other tornadoes indicates that some differences in degree must exist between individual tornadoes.

It is hoped that other high-quality movies of yet unborn tornadoes will be forthcoming so that treatment similar to that provided in this paper can be made.

## ACKNOWLEDGMENTS

The author wishes to express his appreciation to Mr. William A. Hass for his interest in this study and for helpful discussions and comments, and to the several movie photographers for contributing their excellent movies of this tornado from which the raw data for this study were taken.

## REFERENCES

1. Stuart G. Bigler and Edmund P. Segner, Jr., "The Dallas Tornado of 2 April 1957, Raw Data Report," *Scientific Report* No. 2 on Contract Cwb–9116, Department of Oceanography and Meteorology, The Agricultural and Mechanical College of Texas, College Station, Tex., August 1957. (See pp. 193–230.)
2. H. R. Byers and R. R. Braham, *The Thunderstorm*, U.S. Weather Bureau, Washington, D.C., June 1949, 282 pp. (pp. 32–33).
3. Frank B. Dinwiddie, "Waterspout-Tornado Structure and Behavior at Nags Head, N.C., August 12, 1952," *Monthly Weather Review*, vol. 87, No. 7, July 1959, pp. 239–250.
4. Tetsuya Fujita, "A Detailed Analysis of the Fargo Tornadoes of June 20, 1957," *Research Paper* No. 42, U.S. Weather Bureau, Washington, D.C. (in press). (See Chap. 4.)
5. R. G. Beebe, "The Life Cycle of the Dallas Tornado," pp. 3–51 of "The Tornadoes at Dallas, Tex., April 2, 1957," *Research Paper* No. 41, U.S. Weather Bureau, Washington, D.C., 180 pp. (in press).
6. U.S. Weather Bureau, *Meteorology and Atomic Energy*, U.S. Atomic Energy Commission, July 1955, 163 pp. (p. 22).
7. W. H. Hoecker, Jr., "The Dimensional and Rotational Characteristics of the Tornadoes and Their Cloud System," pp. 53–113 of "The Tornadoes at Dallas, Tex., April 2, 1957," *Research Paper* No. 41, U.S. Weather Bureau, Washington, D.C., 180 pp. (in press).

# Weather Note

## JET CONDENSATION TRAIL SHADOWS

DONALD H. LOKKE

4756 Staples Ave., Fort Worth, Tex.

Jet condensation trails are a common occurrence over most of the United States. During the years of 1955 and 1956, shadows of jet condensation trails were observed and photographed on two occasions in northeastern Kansas. The shadows were noted at noon on November 1, 1955, at Lawrence, Kans., and again prior to sunset on June 14, 1956, west of Lecompton, Kans.

The accompanying photographs record the observations of November 1, 1955, when numerous contrails were left as jet planes swept across the sky. The point of observation was located at the western edge of the University of Kansas campus in Lawrence, Kans., at approximately 38°57′30″ N., 95°15′ W. Both photographs were taken with a Leica camera with 50-mm. Elmar lens; f/9 at 1/60 sec., 35-mm. Kodachrome film.

FIGURE 1.—Looking in a westerly direction from the University of Kansas campus in Lawrence, Kans., at 11:58 a.m. (estimated) CST, on November 1, 1955. Shadow is located to the right of jet condensation trail.

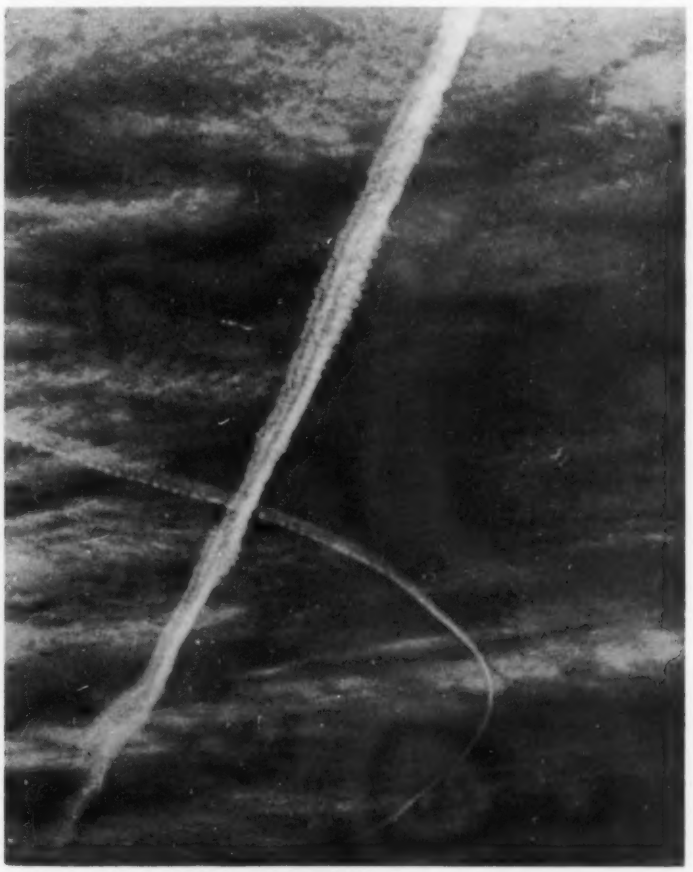

FIGURE 2.—Looking in a west-northwesterly direction from the University of Kansas campus in Lawrence, Kans., at 12:02 p.m. (estimated) CST, on November 1, 1955. Shadow is to the right of the condensation trail.

# TIROS I OBSERVATIONS OF ICE IN THE GULF OF ST. LAWRENCE*

D. Q. WARK AND R. W. POPHAM

U.S. Weather Bureau, Washington, D.C.

[Manuscript received June 7, 1960; revised June 21, 1960]

## ABSTRACT

TIROS I pictures of the Gulf of St. Lawrence, taken during the first days after launch, have clearly revealed areas of ice. The ice patterns found in two series of pictures are mapped. Also shown are aircraft observations of ice made a week earlier and a week later. The results indicate that observations from satellites might contribute to ice surveys.

The first series of photographs taken by TIROS I on April 1, 1960, showed the Gulf of St. Lawrence and its environs. H. Wexler noted gray areas in the Gulf and in the St. Lawrence River which appeared to be ice. At his suggestion an investigation of satellite pictures of this area has been conducted to map the ice and to compare the results with observations made from aircraft by the Canadian Meteorological Service. It was hoped that the results of this study might form the basis for further investigation of the feasibility of utilizing pictures taken from satellites for ice surveys over the water areas of the world.

On April 2 a sequence of narrow-angle pictures was obtained which showed most of the Gulf. A third series,

*This work was supported by the National Aeronautics and Space Administration.

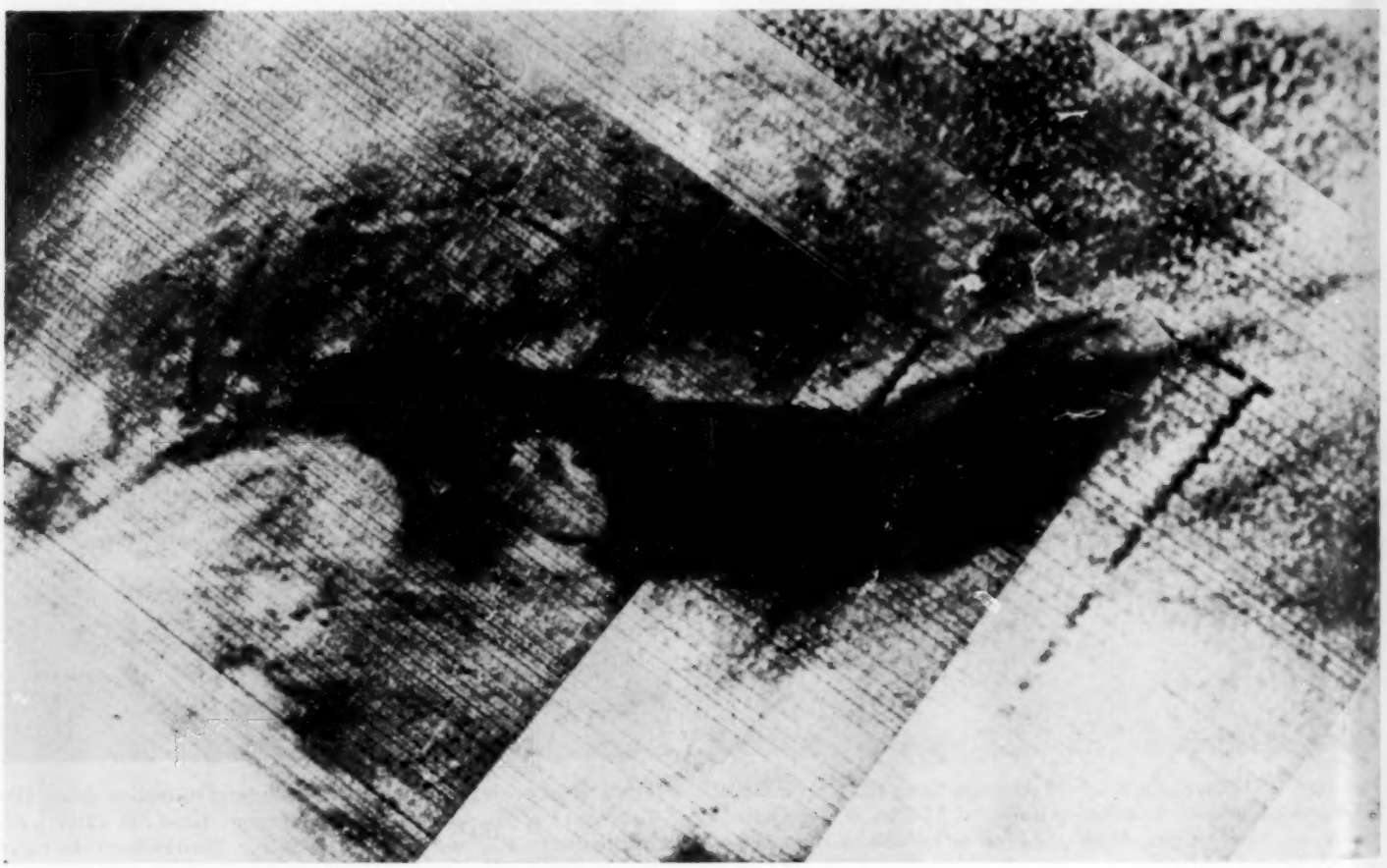

FIGURE 1.—A composite of TIROS I wide-angle photographs taken on April 1, 1960, showing the Gulf of St. Lawrence and environs.


FIGURE 2.—A composite of TIROS I narrow-angle photographs taken on April 2, 1960, showing portions of the Gulf of St. Lawrence and environs.

554818—60——3

taken with the wide-angle camera, as was the original series, also showed the Gulf, but from a greater distance. This time-sequence of pictures over 48 hours has allowed deductions not possible from a single series.

Figure 1 shows a composite of wide-angle photographs taken at about 1500 GMT on April 1. Labrador and Quebec are seen as the gray area in the upper part of the photograph; Newfoundland is on the right; the St. Lawrence River is on the left; the lower part is cloud cover over the southern half of the Gulf. The Gaspé Peninsula and Anticosti Island can be distinguished. The synoptic map at this time showed a large high pressure system in northern Canada centered over Hudson Strait. A frontal system ran south of the High through a weak Low over southeastern Newfoundland, then southwestward through another weak Low off the New England coast. New Brunswick, the lower part of the Gulf, and most of Newfoundland were overcast, while the southern shore of Quebec Province reported mostly scattered clouds. From figure 1 it can be seen that the northern part of the Gulf was clear.

The dark areas are mainly water, while the light areas are mostly land or clouds. In the upper right-hand corner is the Strait of Belle Isle between Labrador and Newfoundland. The grayness in the Strait indicates that it is probably ice-covered. Extending southwestward from the Strait, parallel to but off the coast, is another thin streak of ice which broadens. The main band continues parallel to the coast to the northeastern shore of Anticosti Island, and a branch extends southward between Anticosti Island and Newfoundland to the edge of the clouds. A bright patch can be seen around the eastern end of the island and another just south of the island blends with the clouds. A U-shaped ice pattern can also be readily identified jutting into the St. Lawrence River from the northern coast of the Gaspé Peninsula. Other patterns of ice can be seen just south of the Strait of Belle Isle near Newfoundland.

Figure 2 is a composite of narrow-angle pictures taken at about 1430 GMT on April 2. Newfoundland is on the right; Anticosti Island is in the upper center; the Gaspé Peninsula and the St. Lawrence River are in the lower left. Approximate latitude and longitude lines are shown. The front of the previous day had moved well out to sea, and a high pressure ridge extended southward from the High in northern Canada. The lower St. Lawrence River, the Gulf, and Newfoundland were almost cloudless.

This composite consists of pictures read out directly from the satellite when it was close to the horizon of the monitoring station. The angle of view is quite oblique,

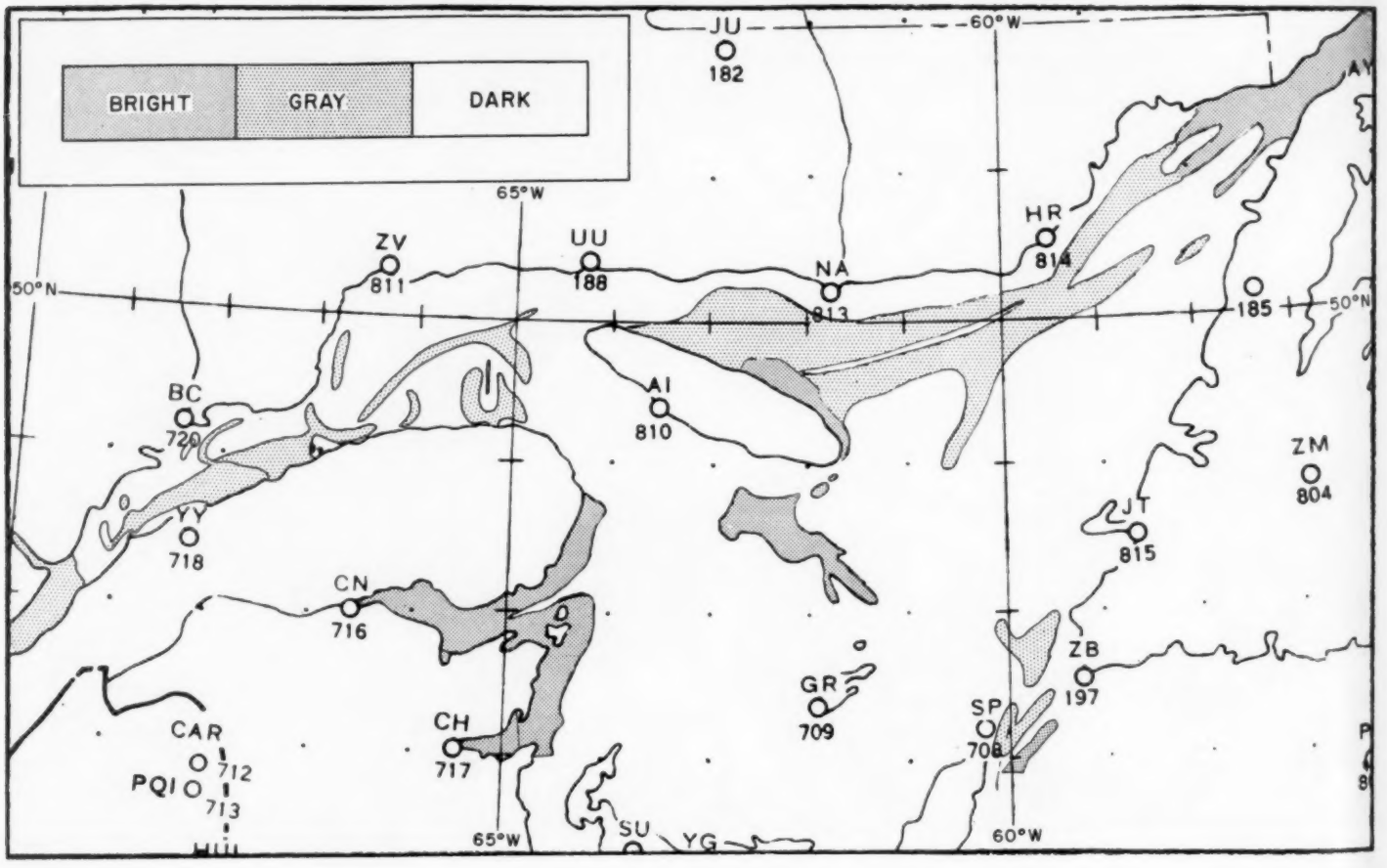


FIGURE 3.—Analysis of ice shown in figures 1 and 2.

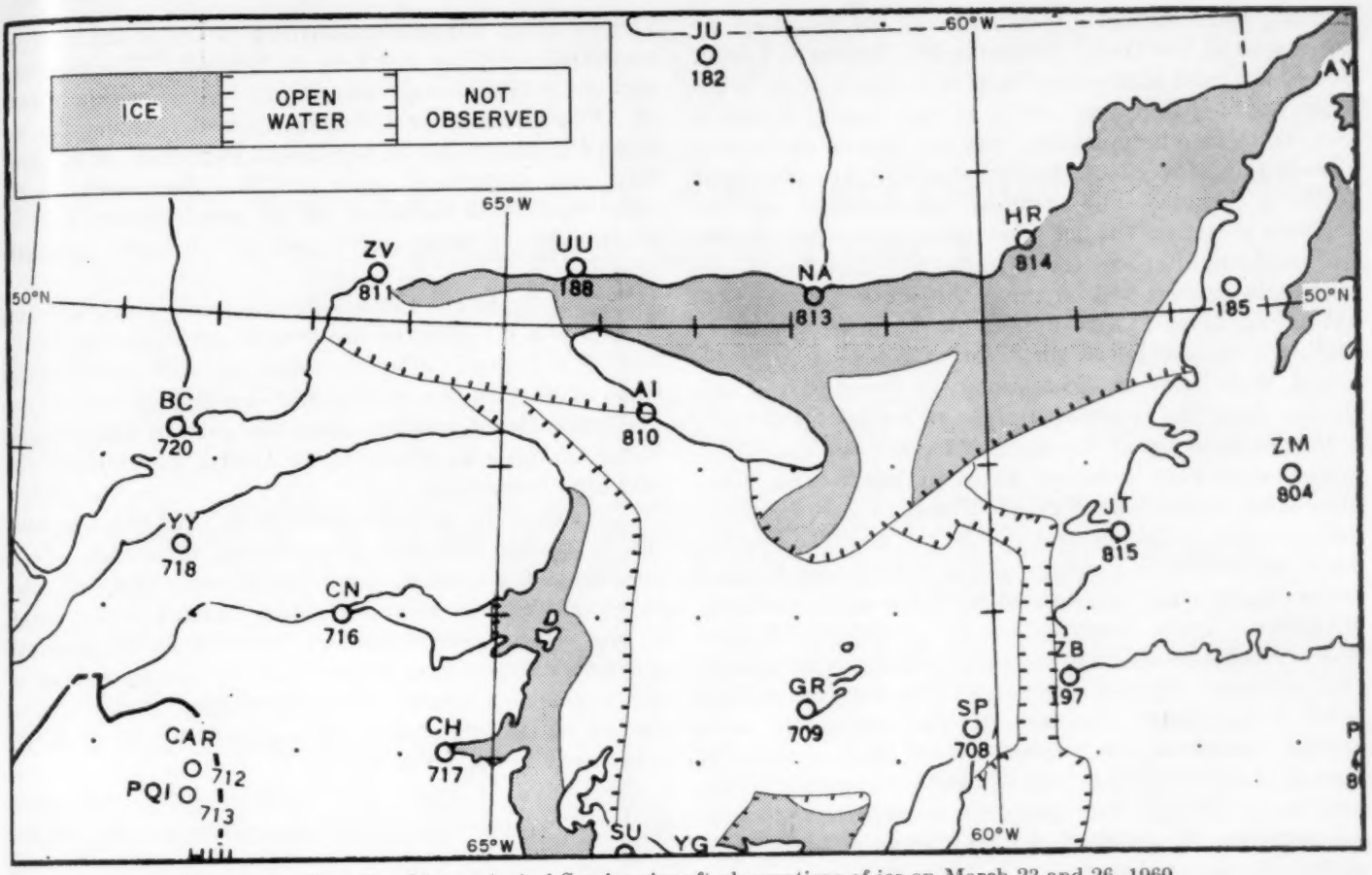


FIGURE 4.—Canadian Meteorological Service aircraft observations of ice on March 23 and 26, 1960.

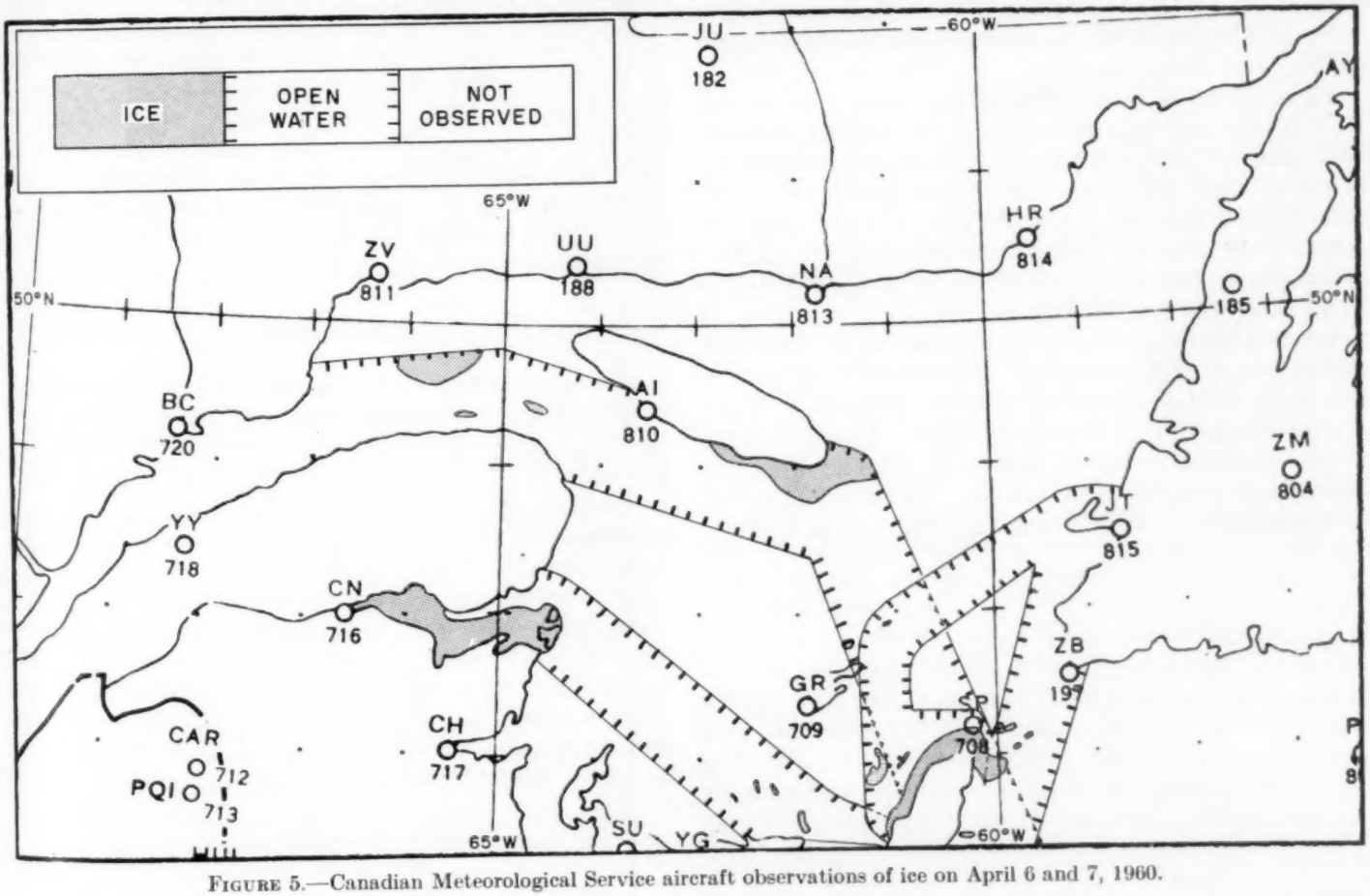


FIGURE 5.—Canadian Meteorological Service aircraft observations of ice on April 6 and 7, 1960.

resulting in considerable foreshortening, as indicated by the shapes of the Gaspé Peninsula and Anticosti Island. One of the most interesting features in this picture is the large bright patch just south of the island, which is believed to be a large ice floe that has broken away from a pack along the island, carried south by the persistent northerly winds. The general configuration of the northern portion of the floe seems to support this hypothesis. Although not so clear as in figure 2, the floe is also evident in figure 1 and on the pictures taken on April 3, not shown here. There appears to be dense, probably pack, ice on the lower northeastern shore of Anticosti Island, while loose ice exists along the upper part of this shore. Near the upper edge of figure 2 at about 60° W., is the southern tip of the band of ice seen in figure 1 to extend southward between Anticosti Island and Newfoundland to the clouded area. The St. Lawrence River from the city of Quebec (not visible, but near the extreme lower left corner) is partially obscured by a thin layer of cirrus clouds, which ends about 80 to 100 miles northeast of Quebec. From there to about 49° N. the river is more clearly visible, with loose ice appearing in indistinguishable patterns. Beyond this point and along the northern coast of the Gaspé Peninsula the ice appears in more dense, curved streaks. From Gaspé Bay southward toward Miramichi Bay the shoreline appears highly reflective. Chaleur Bay looks ice-covered, except near the entrance. Part of Gaspé Bay appears to be open water. Some elongated streaks appear off the southwestern tip of Newfoundland, including one bright streak. The rest of the Gulf contains a few less clearly visible, more diffuse patterns.

Figure 3 shows an analysis of the water areas in the Gulf of St. Lawrence, derived from the satellite information contained in figures 1 and 2. The dense dots indicate areas of high reflectance and, presumably of highly reflecting ice; the open dots indicate gray areas, which are presumed to be ice areas of medium reflectance; unmarked areas appear dark and are interpreted as open water or ice areas of very low reflectance.

Figure 4 shows ice conditions as observed on March 23 and 26 from Canadian aircraft. No attempt was made in this figure to distinguish the type or the density of ice; only open water or ice have been shown. The boundaries of the observed areas are indicated. The anvil-shaped area of open water east of Anticosti Island was observed by the satellite, as shown in the analysis and in figure 1. The ice along the southeastern tip of the island may be associated with the floe seen in figure 2. The northern part of the Gulf was almost entirely ice-covered on March 23. Observations on the 26th showed considerable ice along the eastern tip of the Gaspé Peninsula, in Chaleur Bay, and southward along the New Brunswick coast. Open water was indicated off the southwestern part of Newfoundland, then northwestward toward Anticosti Island.

Figure 5 shows aircraft-observed ice conditions on April 6 and 7. Most of the area observed on these days was open water, although some ice still remained in Chaleur Bay, on the southeastern tip of Anticosti Island, and in scattered patches along the path of observation. Much of the area observed on April 7 was outside the satellite photographs.

The sensitivity of the television of TIROS I has been set to render the best reproduction of clouds. It is possible that one might prefer greater sensitivity in order to reveal ice areas which are nearly as dark as the water. In the present case it has been found that the range of grayness extends from white down to the noise level of the system. A greater sensitivity might reveal more of the ice of low reflectance while permitting ice of higher reflectance to appear to be white.

On the other hand, these pictures have been taken under unfavorable circumstances, looking at very oblique angles. Pictures taken in the vertical are generally much superior and would reveal more.

It should be mentioned that the problem of distinguishing between ice and clouds is not severe. The existence of pictures on three days has permitted a positive identification of the large floe as ice rather than cloud. A satellite is capable of at least daily observations and only persistent thick clouds should limit knowledge of ice conditions. Ice can definitely be observed in photographs from satellites and it is hoped that in the future satellites can contribute to ice surveys.

ACKNOWLEDGMENT

We thank the Director of the Meteorological Service of Canada for furnishing the ice survey charts, and also members of the Division of Oceanography, U.S. Navy Hydrographic Office, and Mr. A. E. Sik of the Forecasts and Synoptic Reports Division, U.S. Weather Bureau, for assistance in assembling the ice data. We are particularly indebted to H. Wexler for his suggestions and comments.

# HIGH ALTITUDE WIND DATA FROM METEOROLOGICAL ROCKETS

LCDR. C. L. ARMSTRONG, USN* and LT. (jg) R. D. GARRETT, USN*

[Manuscript received March 29, 1960; revised May 16, 1960]


## ABSTRACT

This paper presents a preliminary summary of results obtained from meteorological rocket firings made by the United States Navy from Point Mugu, Calif., during the fall of 1959 and the winter of 1960.

Although certain problems were encountered during these initial firings, it is felt that the wind data derived is as complete and as reliable as present acquisition, read-out, and instrumentation techniques will permit.

The data compare favorably with those obtained from high-level balloon soundings and tend to support previous ideas on wind flow in the mesosphere.


## 1. INTRODUCTION

In the fall of 1959 the Inter-Range Meteorological Working Group (IRMWG) established a Meteorological Rocket Network [1] and initiated a synoptic schedule calling for daily launches during one month of each season. Because of safety and instrumentation considerations, the initial network of stations was limited to six missile ranges. Point Mugu, Calif. (Pacific Missile Range), as one of the participating stations, accomplished regularly scheduled firings in October and November of 1959 and January and February 1960. Although the art of using meteorological rockets, motivated by requirements for winds to very high altitudes, has just begun to be exploited, it is felt that great potential for further progress is evident.

## 2. ROCKETS

Three types of meteorological probes have been used thus far. The ARCAS (all-purpose rocket for the collection of atmospheric soundings) is a single-stage, unguided, solid propellant vehicle with an altitude capability of 210,000 feet. A 15-ft. metalized parachute (ejected at apogee) serves as a radar target for computing wind drift and also carries a 4- to 5-lb. instrument package that telemeters temperature data back to a standard GMD rawinsonde station utilizing a 1680 mc. transmitter. LOKI I and LOKI II rockets are also unguided, solid propellant vehicles but have a second stage consisting of an unpowered dart. The LOKI I dart contains an 8-ft. mylar parachute while the LOKI II dart usually contains S-band radar chaff. Wind data are obtained by radar track of the targets (instrumented darts are not yet available). The LOKI I and LOKI II rockets have altitude capabilities of approximately 110,000 ft. and 225,000 ft., respectively. A summary of the meteorological rocket firings at Point Mugu, from which data were obtained, is presented in table 1. Tracking support was provided by SCR 584 and FPS–16 radars.

## 3. RESULTS

Figures 1 and 2 are time cross sections depicting wind data obtained during fall and winter respectively. Height in kilometers and thousands of feet is shown on the ordinate and firing days are indicated on the abscissa. The standard wind plotting system (50 kt. per flag, 10 kt. per full barb, 5 kt. per half barb) is utilized to show wind direction and speed.

It is noteworthy that the rocket observations confirm the polar front jet stream in the upper troposphere and the familiar wind speed minimum above the tropopause near 70,000–80,000 ft. Figure 1 actually reveals a weak zone of easterlies at these levels during late October. Figure 2 shows this same interesting breakdown in the normal westerly flow during early February with a clearly defined easterly maximum occurring on the 1st and 2d at 100,000–110,000 ft.

Figure 3 shows the mean zonal winds plotted against altitude using data obtained from both the fall and winter series. This graph is quite interesting in that it shows the rapid increase of the zonal westerlies in the mesosphere. In spite of the fact that no corrections have been applied for wind response delay at target deployment, the mesospheric maximum is apparently located near the average peak altitude being achieved by the rockets. The few

*Assigned to Pacific Missile Range Weather Center, Point Mugu, Calif. The opinions expressed herein are the authors' own and do not necessarily reflect the views of the Navy Department.

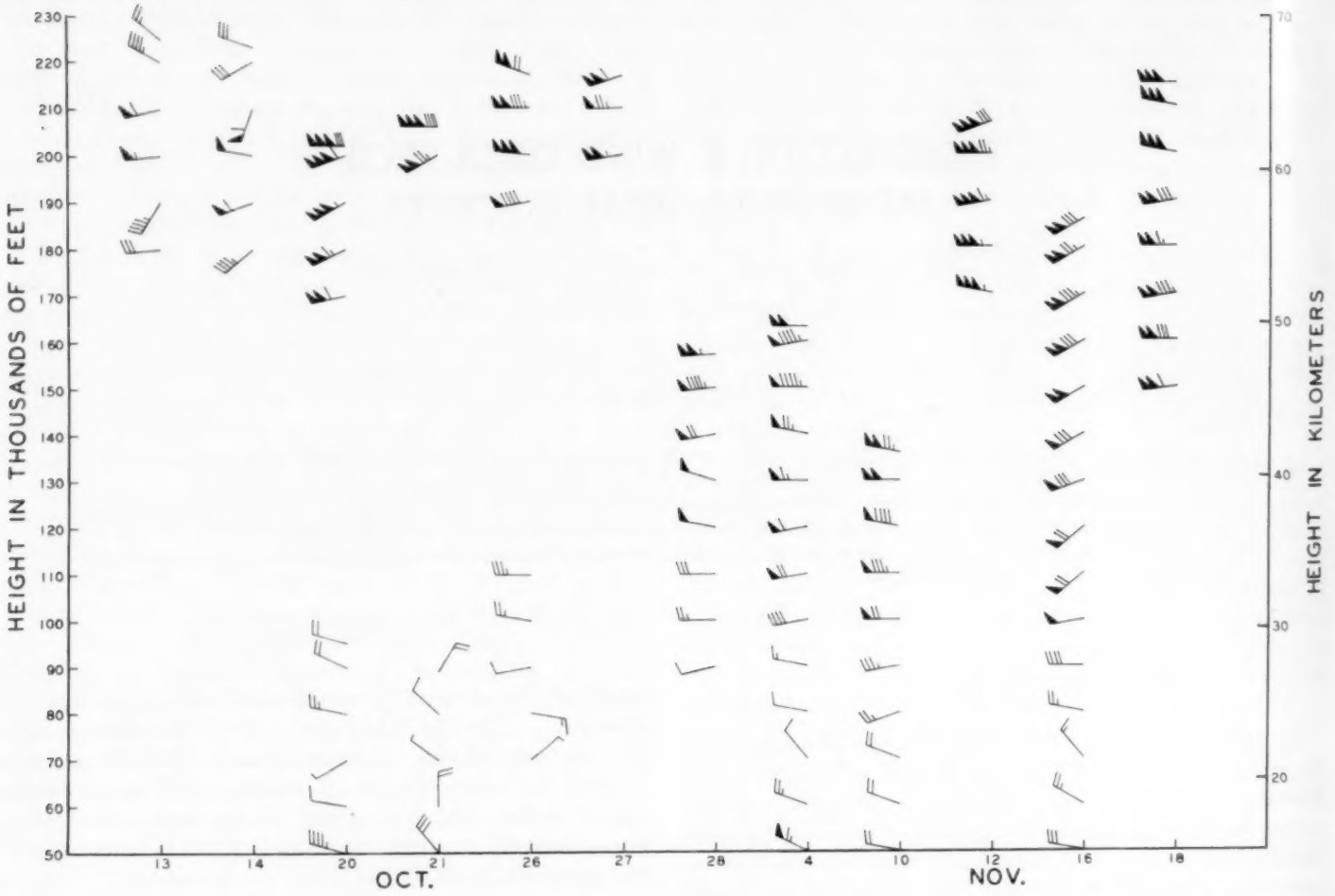


FIGURE 1.—Time cross section showing wind data obtained by rocketsonde in October and November 1959 series, Pacific Missile Range, Point Mugu, Calif.

TABLE 1.—*Meteorological rocket summary. Pacific Missile Range, Point Mugu, Calif.*

| Fall series | | | | Winter series | | | |
|---|---|---|---|---|---|---|---|
| Date | Vehicle | Peak altitude (Thousands of feet) | Interval sampled (Thousands of feet) | Date | Vehicle | Peak altitude (Thousands of feet) | Interval sampled (Thousands of feet) |
| Oct. 13, 1959 | LOKI II | 231 | 225–178 | Jan. 15, 1960 | LOKI I | 123 | 114–50 |
| Oct. 14, 1959 | LOKI II | 227 | 223–173 | Jan. 18, 1960 | ARCAS | 196 | 176–54 |
| Oct. 20, 1959 | LOKI II | unknown | 201–170 | Jan. 21, 1960 | LOKI I | 110 | 110–58 |
| Oct. 20, 1959 | LOKI I | 116 | 95–50 | Jan. 22, 1960 | ARCAS | 188 | 173–48 |
| Oct. 21, 1959 | LOKI II | 210 | 206–192 | Jan. 25, 1960 | LOKI II | unknown | 212–163 |
| Oct. 21, 1959 | LOKI I | 102 | 102–27 | Jan. 26, 1960 | LOKI I | 128 | 104–50 |
| Oct. 26, 1959 | LOKI II | unknown | 218–189 | Jan. 28, 1960 | LOKI I | 113 | 111–50 |
| Oct. 26, 1959 | LOKI I | unknown | 115–70 | Feb. 1, 1960 | ARCAS | 150 | 116–36 |
| Oct. 27, 1959 | LOKI II | unknown | 216–195 | Feb. 2, 1960 | LOKI I | 115 | 110–70 |
| Oct. 28, 1959 | ARCAS | 168 | 157–90 | Feb. 3, 1960 | ARCAS | 168+ | 144–41 |
| Nov. 4, 1959 | ARCAS | 195 | 163–40 | Feb. 4, 1960 | ARCAS | 185 | 160–85 |
| Nov. 10, 1959 | ARCAS | 202 | 136–43 | Feb. 5, 1960 | ARCAS | 148 | 138–40 |
| Nov. 12, 1959 | LOKI II | 220 | 207–165 | Feb. 8, 1960 | ARCAS | 180 | 162–23 |
| Nov. 16, 1959 | ARCAS | 192 | 186–48 | Feb. 11, 1960 | LOKI I | 114 | 114–49 |
| Nov. 18, 1959 | LOKI II | 217 | 215–148 | Feb. 15, 1960 | ARCAS | 202 | 183–46 |
| | | | | Feb. 16, 1960 | ARCAS | 165 | 150–45 |
| | | | | Feb. 17, 1960 | ARCAS | 200 | 196–47 |

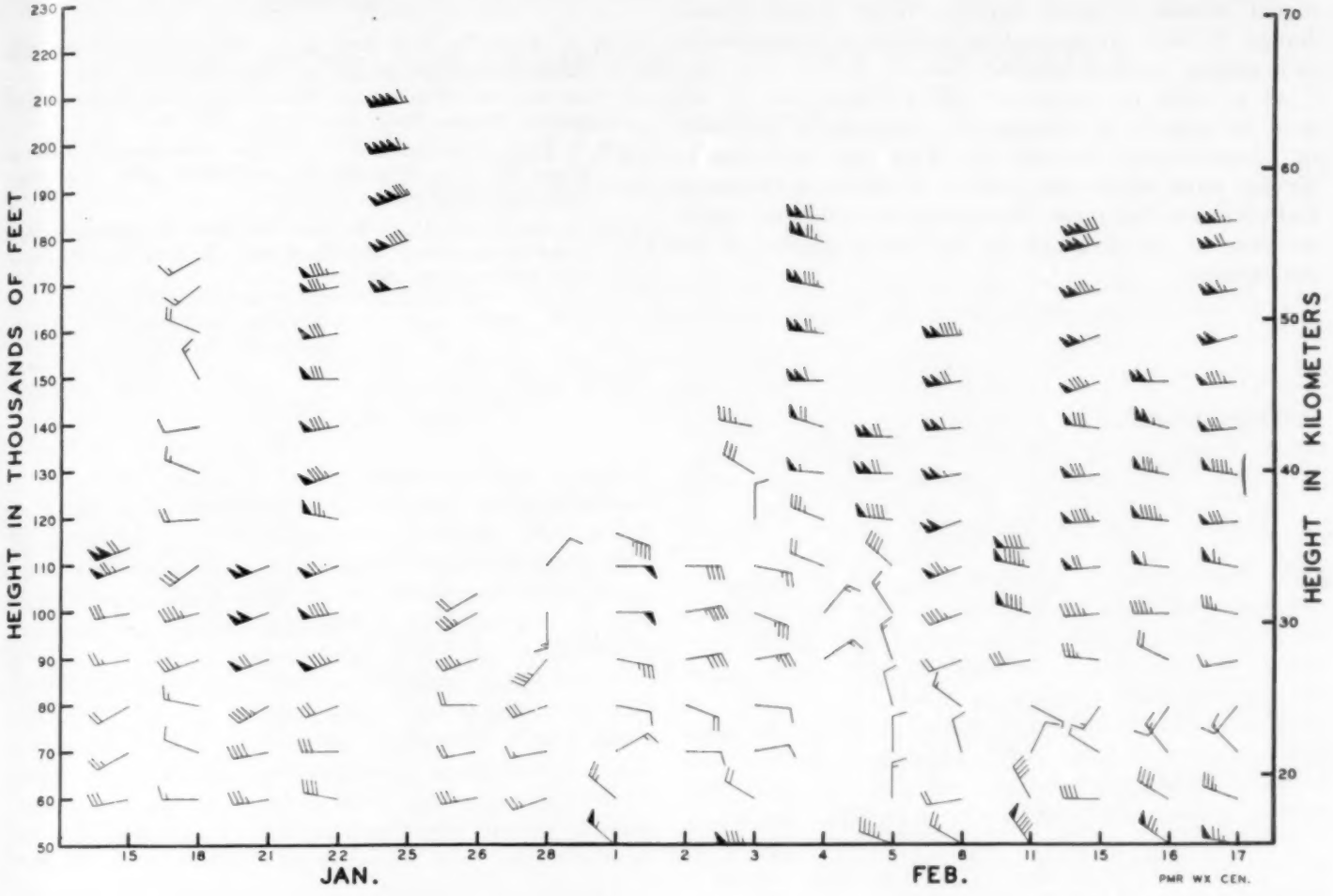


FIGURE 2.—Time cross section showing wind data obtained by rocketsonde in January and February 1960 series, Point Mugu, Calif.

soundings over 210,000 ft. indicate a decrease in speed above that height.

Fortunately, Point Mugu is located at the same latitude as that estimated for the mesospheric jet core. There is a striking resemblance between the profile shown in figure 3 and the distribution postulated by Pant [2].

## 4. CONCLUSION

The fall and winter series of firings have provided a large amount of wind data in regions beyond the capability of balloons. Instrumental difficulties, primarily with sensors, have precluded collections of equal amounts of temperature data up to 200,000 ft. Some soundings are available [3] however, and more are expected from an improved instrument package being developed at Point Mugu. The next in the series of seasonal launches, the spring series, will take place during April and May of 1960.

Data derived from rockets fired from each of the stations in the network are being forwarded to the U.S. Army

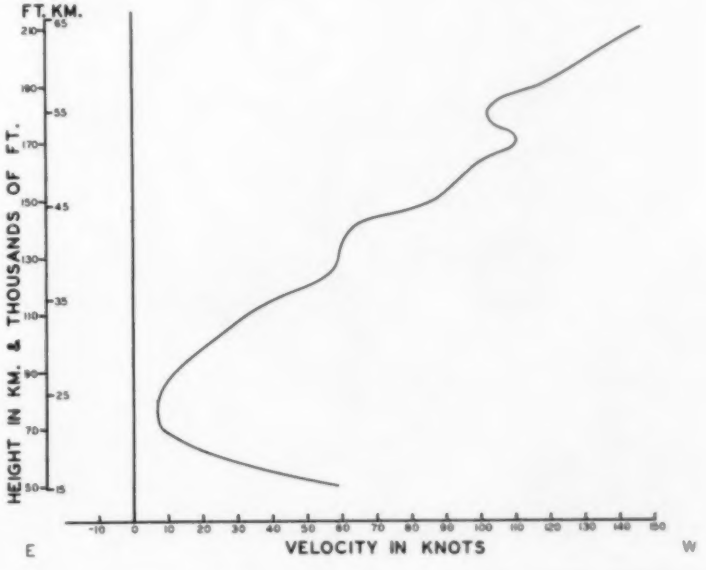


FIGURE 3.—Mean zonal wind, Point Mugu, Calif., obtained from data for fall and winter 1959–60 meteorological rocket program.

Signal Missile Support Agency, White Sands Missile Range, N. Mex., for evaluation and further dissemination to interested research groups.

As a result of improved ARCAS hardware, it will soon be possible to increase the rocketsonde capability to approximately 300,000 ft. This will undoubtedly divulge data which will further whet the appetites of meteorologists for more information to aid in an understanding of the structure of the upper reaches of the atmosphere.

REFERENCES

1. W. L. Webb, W. E. Hubert, R. L. Miller, and J. F. Spurling, "Initiation of Meteorological Rocket Network," to be presented at the 187th National Meeting, American Meteorological Society, Eugene, Oreg., June 14–16, 1960.
2. P. S. Pant, "Circulation in the Upper Atmosphere," *Scientific Report* No. 1 on Contract No. AF19(604)–1006, New York University, May 1955.
3. D. E. Ogden and D. B. Swinton, "ARCAS Temperature Data in the Mesosphere," *Monthly Weather Review*, vol. 88, No. 5, May 1960, pp. 191–192.

# ARCAS TEMPERATURE DATA IN THE MESOSPHERE

D. E. OGDEN* and D. B. SWINTON*

Headquarters, Pacific Missile Range, Point Mugu, Calif.

[Manuscript received April 25, 1960; revised June 6, 1960]

## ABSTRACT

The purpose of this paper is to report the preliminary results depicting some of the direct measurements made by sounding rockets at Point Mugu, Calif. The data show good correlation with theoretical standards and high level balloon soundings.

## 1. INTRODUCTION

The Headquarters, Pacific Missile Range initiated active participation in the Meteorological Rocket Network [1] in the fall of 1959. The primary purpose of this network is to collect upper-atmosphere meteorological data on a quasi-synoptic basis by scheduling daily rocketsonde launches for a 1-month period in each season. In the past, a number of rockets (e.g., VIKING, AEROBEE, NIKE-CAJUN, etc.) have been used to gather valuable meteorological information above the heights normally attained by weather balloons. However, all the above mentioned vehicles are relatively complicated, yield "smoothed" data because of their high velocities, and are too expensive to be used on a synoptic basis at a large number of stations. Consequently, they do not meet the need for a simple, relatively inexpensive, semi-mobile rocket sounding system whereby launches can be made on a schedule approaching a synoptic basis without the imposition of overly severe safety limitations.

## 2. THE ARCAS ROCKET

The ARCAS (all-purpose rocket for the collection of atmospheric soundings) is one of the first all-purpose, low-cost rockets used to measure both temperature and winds in the upper atmosphere. It is a single-stage, unguided, solid propellant vehicle with an altitude capability in excess of 200,000 ft. Highly desirable features of the launcher are that it is mobile, has a closed breech, and can be moved and reassembled in four man-hours. Relatively slow acceleration is used to minimize instrumentation shock while a long burning time is used to provide thrust well above the lower, denser atmospheric regions. By utilizing the additional thrust that the closed-breech launcher provides, the rocket accelerates continuously to a burn-out speed of 3,865 ft. sec.$^{-1}$.

The problem of chute design was formidable; however, recent firings indicate successful deployment at altitudes in excess of 200,000 ft. At present, a 15-ft., mylarized chute (ejected at apogee) is used both as a radar target for obtaining winds, and as a carrier for the telemetering package. Fall rates vary from in excess of 20,000 ft. min.$^{-1}$ at 200,000 ft. to less than 500 ft. min.$^{-1}$ in the lower troposphere with a 5-lb. package.

## 3. INSTRUMENTATION

During the first series of firings at Point Mugu, Calif. in the fall of 1959, the so-called "Alpha" package developed by the Missile Geophysics Division, United States Army Signal Missile Support Agency, White Sands, N. Mex. [2], was used as payload. This package was essentially a T304/AMT–4 radiosonde modified to fit in the ARCAS nose cone. Due to numerous technical difficulties, no temperature data were obtained during this series although some excellent wind soundings were made [3].

Prior to the winter (1959–60) series of firings, one of the authors redesigned several of the White Sands Alpha packages; and these ultimately yielded good temperature

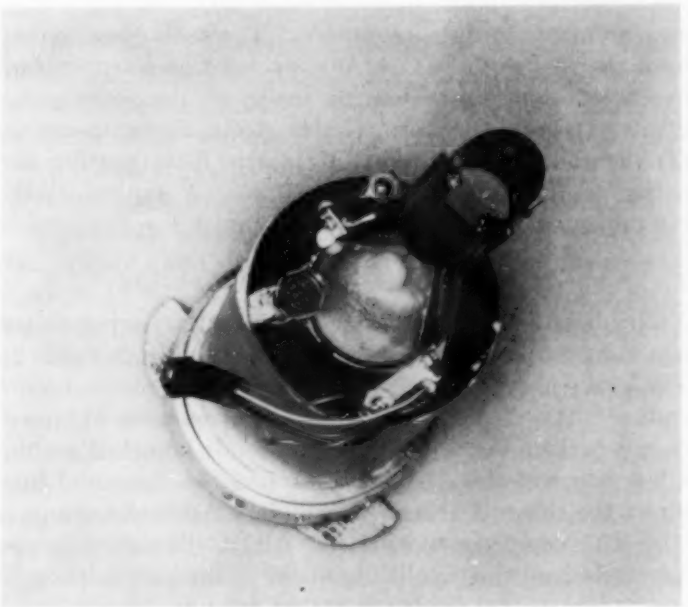

FIGURE 1.—Pacific Missile Range instrument package completely potted in polyurethane just prior to being inserted in nose cone.

*Any opinions expressed by the authors are their own and do not necessarily reflect the views of the Navy Department at large.

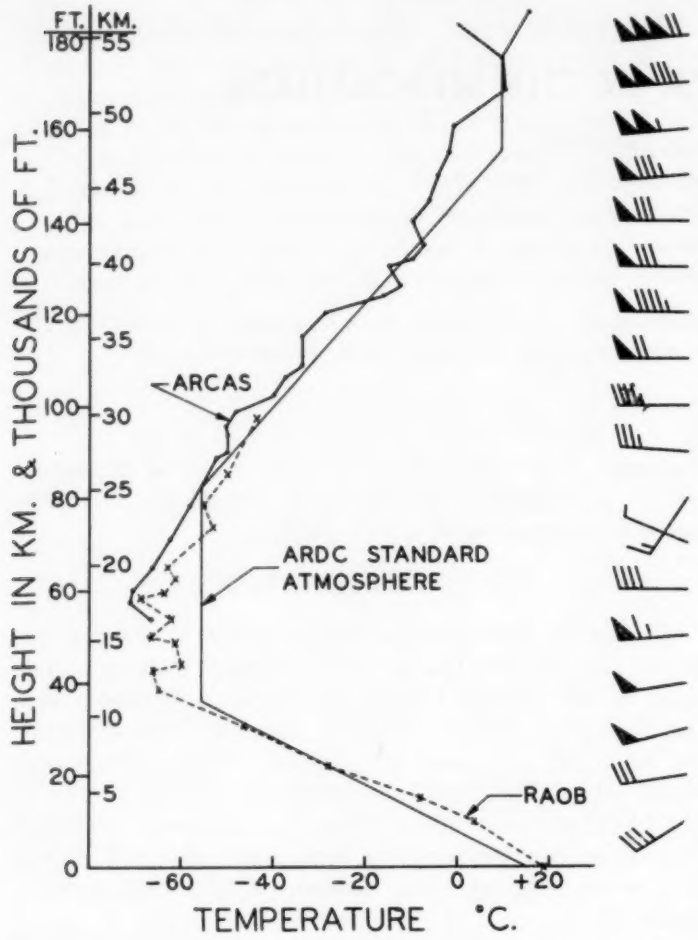


FIGURE 2.—Sounding obtained from ARCAS rocket (heavy solid line) February 15, 1960, compared with that from a balloon-borne AMT–4 radiosonde (dashed line) launched shortly afterward, and with the ARDC standard atmosphere curve (thin solid line).

measurements in the mesosphere. The same glass-coated bead thermistor (VECO 43A6) was used as a sensor, but the most significant changes made in the redesigning involved using: (1) more reliable electronic components, (2) dry-cell batteries, and (3) plastic foam potting for better thermal and shock insulation. A typical PMR instrument package is pictured in figure 1.

## 4. RESULTS

The best sounding obtained during the spring series was made on February 15, 1960, and is shown in figure 2. The heavy solid line represents the ARCAS rocket temperatures; the dashed line depicts temperatures obtained from a balloon-borne AMT–4 radiosonde launched within a few hours of the ARCAS firing and the thin solid line shows the theoretical ARDC Standard Atmosphere curve [4]. The comparison with the ARDC Standard is remarkable, and the paralleling of the radiosonde (although on the lower side) is also most encouraging, especially in the vicinity of the tropopause. Lift-off occurred at 1914 GMT and the radiosonde was launched at 2155 GMT.

TABLE 1.—*A summary of* ARCAS *temperatures for three firings in February 1960*

| Altitude | Feb. 1, 1960 | Feb. 5, 1960 | Feb. 15, 1960 |
|---|---|---|---|
| *feet* | °C. | °C. | °C. |
| 135,000 | −13 | −27 | −7 |
| 130,000 | −20 | −33 | −14 |
| 125,000 | −26 | −34 | −13 |
| 120,000 | −32 | −40 | −25 |
| 115,000 | −30 | −40 | −39 |
| 110,000 | −38 | −41 | −33 |
| 105,000 | −34 | −43 | −37 |
| 100,000 | −45 | −43 | −45 |
| 95,000 | −50 | −45 | −51 |
| 90,000 | −53 | −52 | −50 |

Above 175,000 ft. the ARCAS temperatures were considerably higher than Standard Atmosphere due to the heat generated both from the batteries while the instrument was in the launcher and from skin friction during ascent. Environmental response appeared to be quite rapid, however, and reasonable data resulted after a fall of about 1 minute. Tracking of the ARCAS was terminated as range time had expired.

Two more partial soundings (shortened by battery failure using the PMR package) were obtained on February 1 and 5, 1960. Again the temperature comparisons at levels which overlapped with radiosonde data were very good. A summary of the temperatures available from all these soundings is given in table 1. It is interesting to note, that at the lower levels there was little change during the period covered, while greater fluctuations apparently occurred at higher elevations in the mesosphere.

The soundings of February 1 and 5 were fired at an elevation of 82°, whereas the sounding of February 15 was fired at an elevation of 85°, consequently rather disappointing altitudes were reached.

## 5. CONCLUSIONS

The data collected to date are very sketchy but agree quite well with both radiosonde observations and theoretical curves. There is a hint that we can expect rather large temperature variations in the mesosphere. It is hoped that rapidly improving instrumentation will yield more soundings during the Meteorological Rocket Network spring series in April and May of 1960.

## REFERENCES

1. W. L. Webb, W. E. Hubert, R. L. Miller, and J. F. Spurling, "Initiation of Meteorological Rocket Network," to be presented at 187th National Meeting, American Meteorological Society, June 14–16, 1960, Eugene, Oreg.
2. G. Q. Clark, "Nose Cone Beta," Missile Geophysics Division, U.S. Army Signal Missile Support Agency, White Sands Missile Range, N. Mex., 1959.
3. C. L. Armstrong and R. D. Garrett, "High Altitude Wind Data from Meteorological Rockets," *Monthly Weather Review*, vol. 88, No. 5, May 1960, pp. 187–190.
4. *Handbook of Geophysics for Air Force Designers*, Geophysics Research Directorate, Air Force Cambridge Research Center, Air Research and Development Command, United States Air Force, First Edition, 1957.

# THE WEATHER AND CIRCULATION OF MAY 1960

## Including a Discussion of the Unusual Retrogression of 5-Day Mean Polar Vortices

JAMES F. ANDREWS

Extended Forecast Section, U.S. Weather Bureau, Washington, D.C.

### 1. MEAN CIRCULATION

The monthly mean circulation at 700 mb. for May 1960 (fig. 1) was characterized by strong blocking over much of the higher latitudes of the Northern Hemisphere. In terms of 700-mb. height anomaly, the principal centers of blocking were located over eastern Canada (+320 ft.) and northern Siberia (+370 ft.) with another, somewhat weaker, center over southwestern Alaska (+180 ft.). The effect of this blocking on the mid-latitude planetary circulation was to produce a pattern of truncated trough-ridge systems with rather short wave spacings. The exception to this was in the Pacific where the weaker Alaskan block was associated with a simple zonal pattern and full-latitude mid-Pacific trough (fig. 1).

A further effect of the blocking was to displace the mid-tropospheric westerlies at 700 mb. south of their normal position over most of the western part of the Northern Hemisphere (fig. 2A). The greatest displacement of the zone of maximum west winds was over the eastern United States and western Atlantic, the area south of the Canadian block. Wind speeds at 700 mb. were as much as 7 m.p.s. below normal near Nova Scotia (fig. 2B). Another area of subnormal wind speeds was in the Gulf of Alaska, a manifestation of the Alaskan block. The fastest wind speeds, up to 6 m.p.s. above normal, were found in the eastern Pacific.

The effects of blocking at 700 mb. were also apparent on the monthly mean sea level chart for May (fig. 3). Pressures averaged well above normal over much of the higher latitudes, with centers of greatest departure in northern Siberia (+14 mb.), the western Pacific (+8 mb.), and eastern Canada (+7 mb.). Sea level pressures and 700-mb. heights were both well below normal across most of the United States and Atlantic (figs. 1 and 3), a further indication of the strong blocking in eastern Canada.

### 2. AVERAGE UNITED STATES WEATHER

May was a rather cool month over much of the contiguous United States. Temperatures were generally below normal, except in the central and southern Rocky Mountain States, the Northern Plains, along the California coast, and in the Northeast, where above normal temperatures prevailed (fig. 4A). The greatest negative departures were observed in the Pacific Northwest where temperatures averaged 4° F. below normal. Greatest positive departures were found in the Northeast where Caribou, Maine, reported 9° F. above normal for May. No monthly mean temperature records were established, one reason being that May had two relatively well-defined temperature regimes (see section 3).

The May temperature pattern was well related to the mean circulation pattern. In general the cool weather was associated with below normal 700-mb. heights and westerlies well south of normal across the United States (figs. 1 and 2). The thickness of the layer between 1000 mb. and 700 mb. was also below normal over most of the Nation (fig. 5). The warmth in the Northeast was related to the strong ridge over eastern Canada and associated southeasterly anomalous flow at the surface (fig. 3) and aloft (fig. 1). Thickness values were also above normal in this area.

Figure 4B shows the total precipitation and figure 4C the percentage of normal precipitation for May 1960. Near record amounts fell in the Pacific Northwest where some areas received more than twice their normal totals for the month. Heaviest amounts fell along the coast and at the higher elevations. Mt. Shasta, Calif., with a record dating back to 1888, recorded its greatest snowfall for May, while Stampede Pass, Wash., set a new May record for total precipitation with 9.12 inches.

Precipitation was also heavy in portions of the Mid-West and Middle Atlantic States (figs. 4B, 4C). La Crosse, Wis., experienced its wettest May since observations began in 1873. Near record amounts fell in Green Bay, Wis., Marquette, Mich., and Tulsa, Okla. Areas receiving less than half their normal totals for May were Wyoming, northern and eastern Texas, northwestern Georgia, and central Florida (fig. 4C).

Precipitation, as is usually the case during the warm season, was not too well related to the mean circulation. A strong relationship existed in the Pacific Northwest, however, where cool, wet weather accompanied stronger than normal southwesterly flow from the trough in the eastern Pacific (figs. 1, 2B). Furthermore, the heaviest precipitation fell close to or just north of the zone of maximum wind at 700 mb. (figs. 2, 4B). The band of

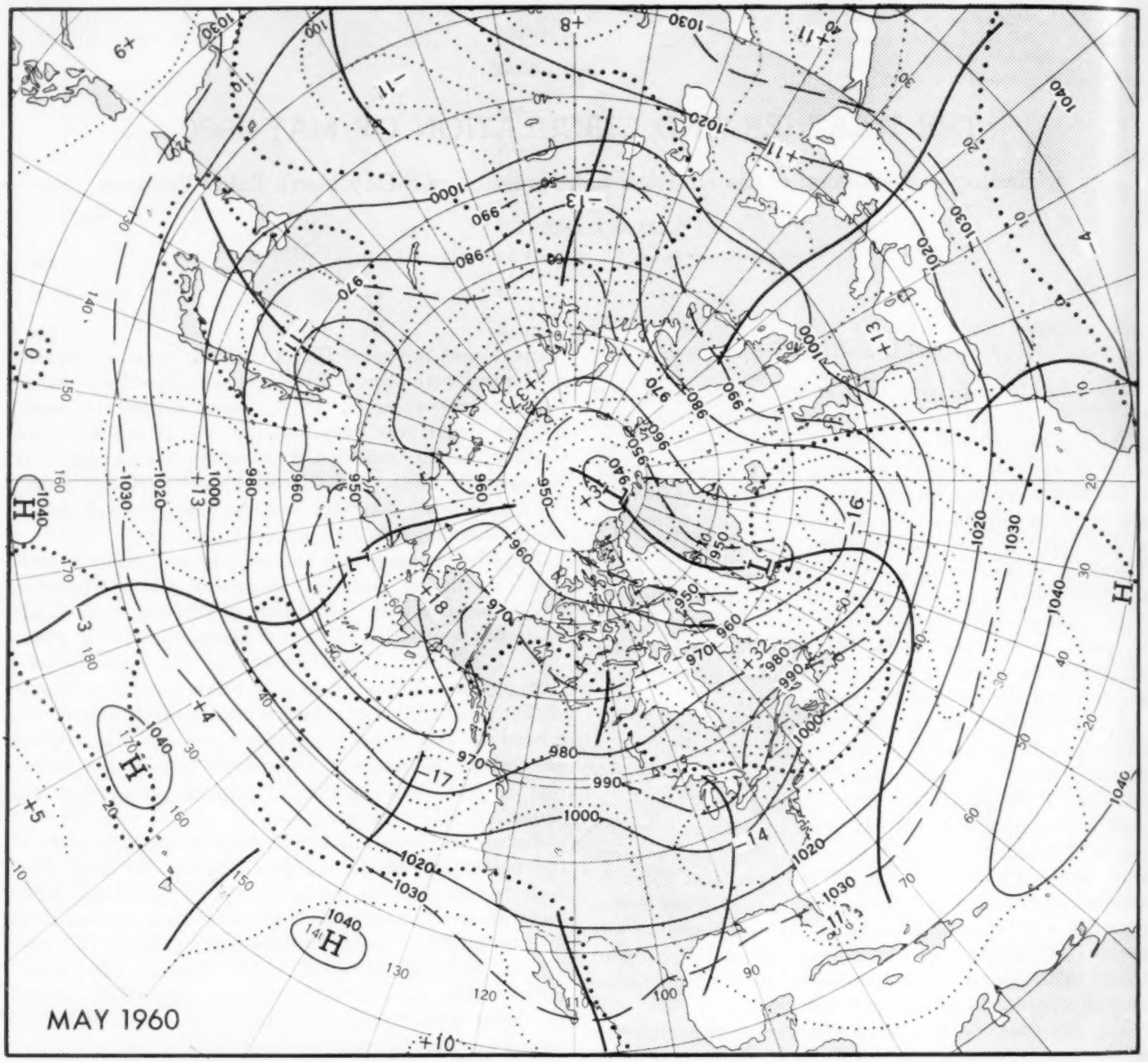


FIGURE 1.—Mean 700-mb. contours (solid) and height departures from normal (dotted), both in tens of feet, for May 1960. Blocking was a prominent feature of the circulation.

precipitation stretching from Nevada to New Mexico, with lower percentages to the north and south (figs. 4B, 4C), appears to bear some relationship to the difluent circulation pattern at 700 mb. (fig. 1). Most of the precipitation in the eastern half of the United States can be associated with the deep mean trough over that area. It is interesting to note, however, that the smaller amounts (and percentages) were observed in the trough itself and generally in the area defined by the −100-ft. departure from normal isoline (figs. 1, 4B, 4C). Amounts were much greater in the surrounding area.

Alaska was unseasonably warm during May with mostly subnormal amounts of precipitation (fig. 4). Both Fairbanks and Juneau experienced their warmest Mays of record, while Yakutat reported its driest May. This warm, dry regime was associated with a strong ridge, above normal 700-mb. heights, and positive thickness in the layer 1000 mb. to 700 mb. (figs. 1, 5).

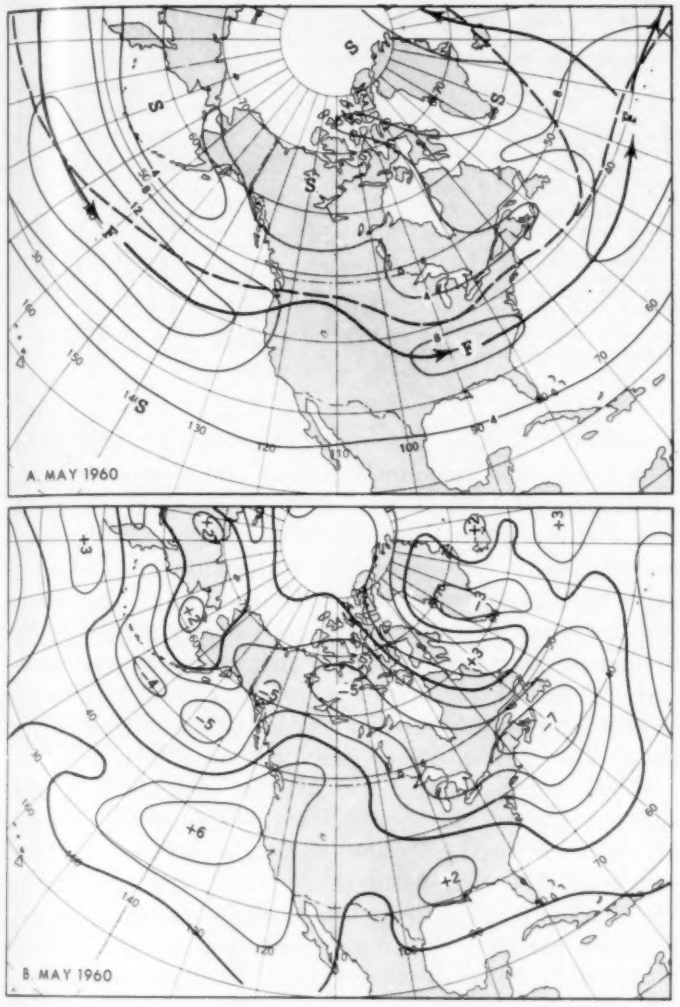


FIGURE 2.—(A) Mean 700-mb. isotachs and (B) departure from monthly normal wind speed (both in meters per second) for May 1960. Solid arrows in (A) indicate axes of primary west wind maxima with the normal position dashed. Because of blocking, the westerlies were displaced to lower latitudes.

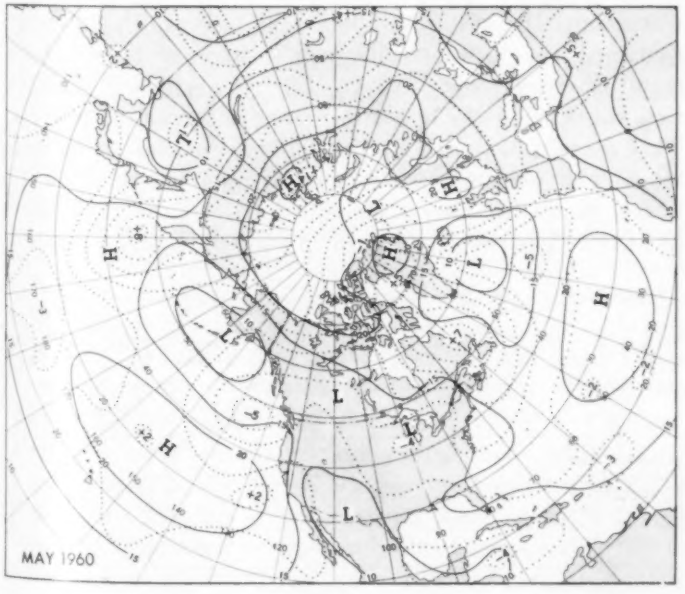


FIGURE 3.—Mean sea level isobars (solid) and their departures from normal (dotted), both in millibars, for May 1960. Excess of pressure at high latitudes and deficit at low latitudes were associated with high-latitude blocking.

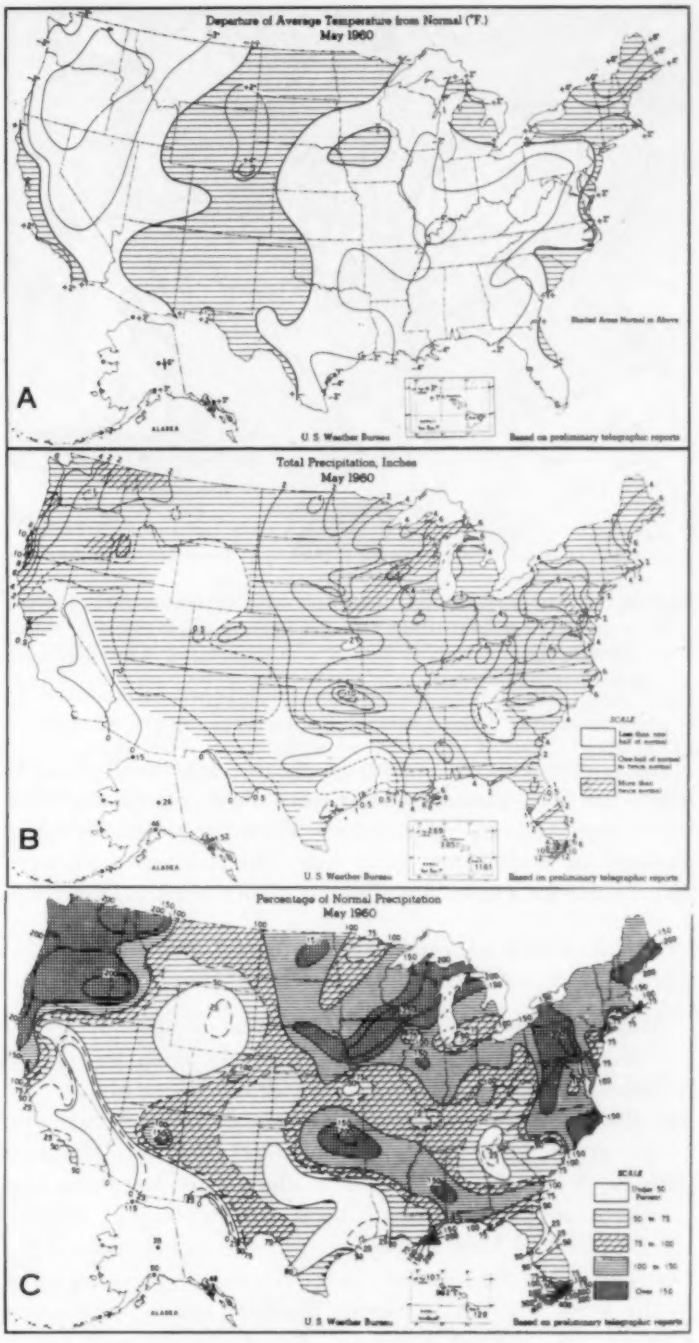


FIGURE 4.—(A) Departure of average temperature from normal (°F.) for May 1960. (B) Total precipitation (inches) for May 1960. (C) Percentage of normal precipitation for May 1960. (From [1].)

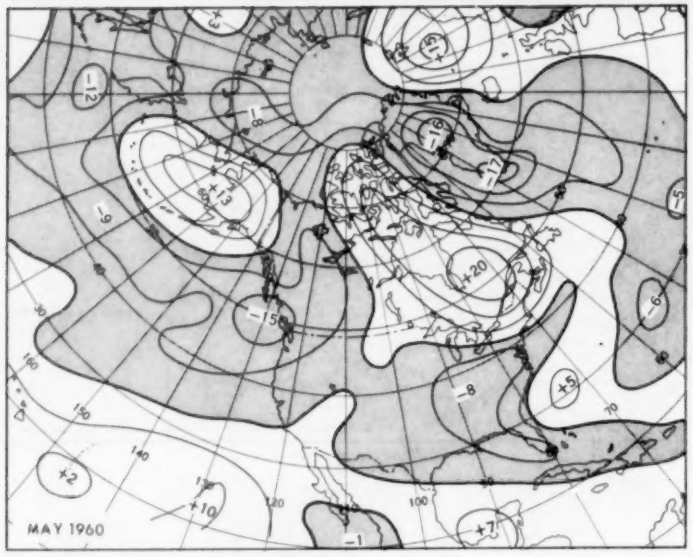


FIGURE 5.—Mean thickness (1000–700 mb.) departure from normal (tens of feet) for May 1960. Below normal thickness over much of the contiguous United States was associated with generally cool surface temperature.

An unusual event occurred in the Hawaiian Islands when the first thunderstorms ever observed during May were reported at Honolulu. They accompanied the passage of a 500-mb. Low over the Islands and were responsible for a new May precipitation record at Honolulu.

## 3. TWO CONTRASTING WEATHER AND CIRCULATION REGIMES

May's weather and circulation was composed of two rather well-defined regimes, particularly with respect to temperature and circulation. In figure 6 are shown the half-month mean circulation patterns at 700 mb. for May 1960, along with the height changes between the two periods, while figures 7 and 8 show the corresponding temperature anomaly and total precipitation. During the first half of May a deep trough was observed over the eastern United States, while ridge conditions predominated in the West (fig. 6A). Strong blocking existed in eastern Canada and helped maintain the westerlies well south of their normal position across eastern North America. The trough was associated with temperatures well below normal over most of the eastern United States, as much as 8° F. in Kentucky and Tennessee (fig. 7A). Only the extreme Northeast, under the influence of a ridge and positive height anomalies, was warm.

Much of the cool weather was the result of a single storm system which developed in the Southwest about May 4. This storm brought heavy rains, hail, and high winds to many sections, tornadoes in Oklahoma and Arkansas, and heavy snowfall in Wisconsin, Upper Michigan, and the eastern slopes of the Colorado Rockies. Dubuque, Iowa, reported 4.38 inches of rain in a 24-hour period on the 5th and 6th, the largest amount in a similar period for any May. Snowfall amounts of 3 to 5 inches were common in much of Wisconsin and Upper Michigan. At Oklahoma City, Okla., a wind speed of 72 m.p.h. exceeded the previous record for any May. As the storm moved slowly northeastward, it became blocked by a large high pressure area over Hudson Bay. Both high and low pressure systems remained nearly stationary for the period May 7–13. Cold air moving southward to the rear of the storm resulted in numerous temperature records being established for the lowest reading so late in the spring. Some of these are listed in table 1.

TABLE 1.—*Late spring minimum temperature records established during May 1960*

| Station | Date | Temperature (° F.) |
|---|---|---|
| Chattanooga, Tenn. | 9 | *35 |
| Madison, Wis. | 12 | 27 |
| Springfield, Mo. | 12 | 30 |
| Abilene, Tex. | 12 | 41 |
| Shreveport, La. | 12 | 42 |
| New Orleans, La. | 13 | *41 |
| Meridian, Miss. | 13 | *38 |
| Montgomery, Ala. | 13 | *42 |
| Apalachicola, Fla. | 13 | *50 |
| Macon, Ga. | 13 | 42 |
| Greenville, S.C. | 13 | 39 |
| Raleigh, N.C. | 13 | 40 |

*Also a record low for any May.

While the East was experiencing temperatures more characteristic of March, the West was enjoying considerably warmer weather during the first half of May (fig. 7A). Much of this warmth occurred during the period May 11–13 when many cities established daily maximum temperature records. In addition, several stations set new maximum temperature records for occurrence so early in the year, as shown in table 2. This extreme warmth, coupled with record cold in the East, resulted from a large-amplitude ridge-trough system.

The circulation reversal which occurred near mid-month was primarily related to establishment of a new trough in the mid-Pacific (fig. 6). This new development in the mid-tropospheric circulation effectively shortened the wavelength between the planetary waves, thus forcing eastward the downstream trough-ridge systems. As a result the trough over eastern North America was replaced by a ridge, while the opposite change occurred in the West. This transition in the mean 700-mb. circulation at mid-month can, perhaps, best be seen by reference to figure 6C, which shows the height changes between the two halves of May. The rather uniform spacing of change centers in

TABLE 2.—*Early season maximum temperature records established during May 1960*

| Station | Date | Temperature (° F.) |
|---|---|---|
| Pocatello, Idaho | 11 | 90 |
| Helena, Mont. | 12 | 88 |
| Billings, Mont. | 12 | 94 |
| Sheridan, Wyo. | 12 | *95 |
| Salt Lake City, Utah | 12 | 92 |
| Winslow, Ariz. | 12 | 94 |

*Ties record for May.

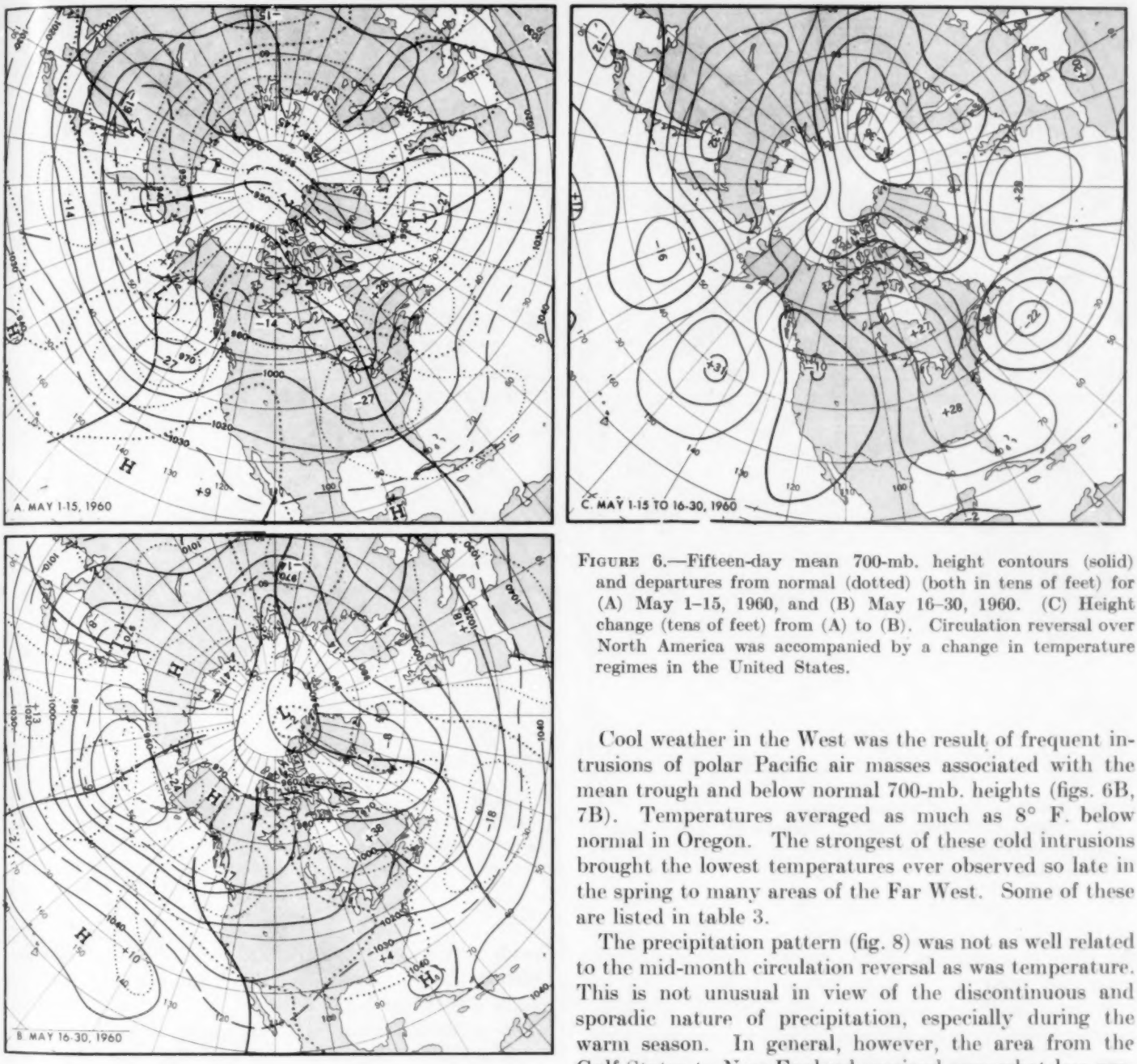


FIGURE 6.—Fifteen-day mean 700-mb. height contours (solid) and departures from normal (dotted) (both in tens of feet) for (A) May 1–15, 1960, and (B) May 16–30, 1960. (C) Height change (tens of feet) from (A) to (B). Circulation reversal over North America was accompanied by a change in temperature regimes in the United States.

the western part of the hemisphere reflects quite well the complete circulation reversal there.

These changes in circulation were accompanied by an equally pronounced reversal of temperature regimes in the United States (fig. 7). Most of the East experienced a rapid change to warmer, while the West reverted to a cold regime. Because of the persistence of blocking and above normal 700-mb. heights in eastern Canada, the Northeast remained warm for the entire month. Caribou, Maine, established several daily maximum temperature records, and a reading of 91° F. on the 29th was the highest temperature ever observed there so early in the season. Elsewhere in the East the unseasonably warm weather was generally not of a record-breaking nature.

Cool weather in the West was the result of frequent intrusions of polar Pacific air masses associated with the mean trough and below normal 700-mb. heights (figs. 6B, 7B). Temperatures averaged as much as 8° F. below normal in Oregon. The strongest of these cold intrusions brought the lowest temperatures ever observed so late in the spring to many areas of the Far West. Some of these are listed in table 3.

The precipitation pattern (fig. 8) was not as well related to the mid-month circulation reversal as was temperature. This is not unusual in view of the discontinuous and sporadic nature of precipitation, especially during the warm season. In general, however, the area from the Gulf States to New England received somewhat less precipitation during the latter half of May, while the Plains States and Mississippi Valley received more (fig. 8). Heavier amounts also fell along the north Pacific coast as

TABLE 3.—*Late Spring minimum temperature records established during May 1960*

| Station | Date | Temperature (° F.) |
|---|---|---|
| Grand Junction, Colo | 19 | 34 |
| Salt Lake City, Utah | 19 | 31 |
| Albuquerque, N.Mex | 20 | 37 |
| Red Bluff, Calif | 22 | 40 |
| Boise, Idaho | 22 | 28 |
| Portland, Oreg | 22 | 33 |
| Yakima, Wash | 22 | 27 |
| Missoula, Mont | 23 | 26 |

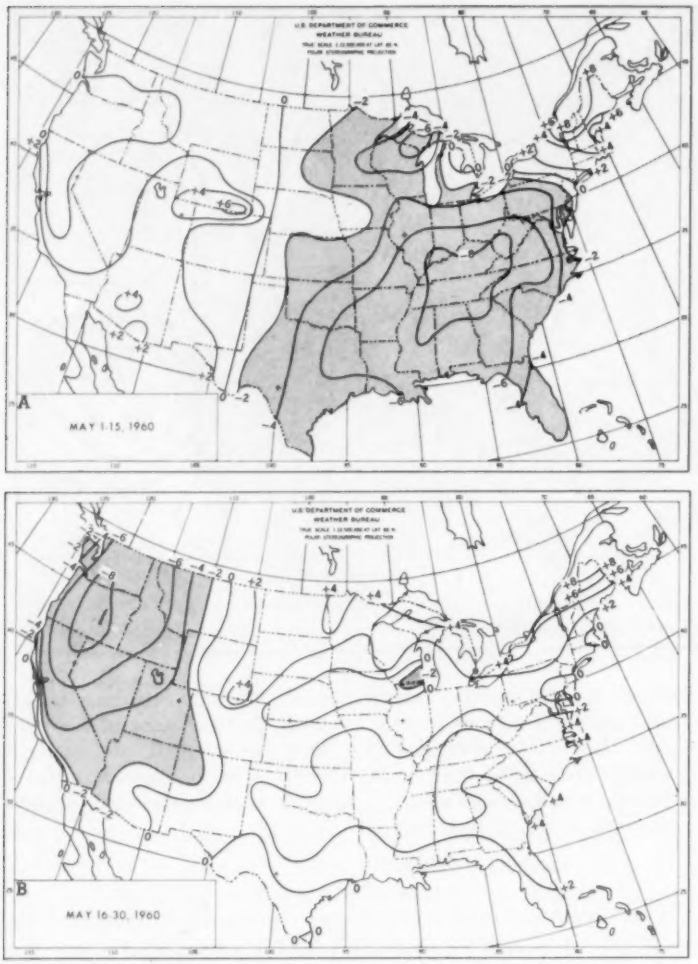


FIGURE 7.—Departure of average temperature from normal (° F.) for (A) May 1–15, 1960, and (B) May 16–30, 1960. Areas of negative departure greater than 2 are stippled. Sharp tempera ture reversal is evident.

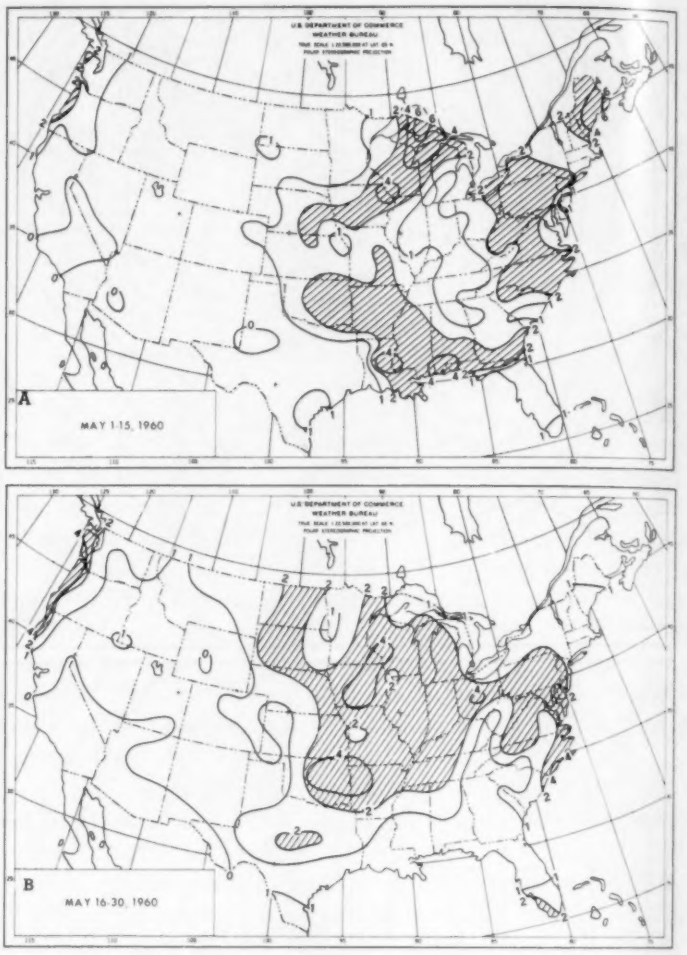


FIGURE 8.—Observed precipitation (approximate) in inches for (A) May 1–15, 1960, and (B) May 16–30, 1960. Areas of amounts greater than 2 inches are hatched.

the mean trough in the eastern Pacific moved toward the coast (figs. 6, 8).

Weather and circulation reversals of this type are not unusual and have been discussed in previous articles of this series. In fact, this is the second consecutive month that this has occurred. Thus, during April-May 1960 a half-month periodicity was observed, primarily in the temperature and circulation patterns in the United States. However, while April [2] was predominantly a warm month, May was cool. This was because the zonal westerlies across the United States were much farther south in May.

## 4. RETROGRESSION OF 5-DAY MEAN POLAR CYCLONIC AND ANTICYCLONIC VORTICES

During May 1960 the polar circulation of the Northern Hemisphere was dominated primarily by two 5-day mean cells, one an anticyclone and the other a cyclone. In figure 9 are shown the tracks of these high and low cells at 700 mb. and sea level, as prepared from 5-day mean charts drawn thrice-weekly in the Extended Forecast Section. Positions shown are one week apart and are plotted on the middle day of the 5-day period.

One striking feature of these tracks is the continuous retrogression of the vortices around the pole. Only the path of the upper-level anticyclone appeared to be discontinuous over the Canadian Arctic near mid-month (fig. 9A). At that time the major 700-mb. High departed from its polar orbit and moved southward into eastern Canada. At the same time, however, the primary surface high pressure area continued in its circumpolar path, although a break-off High (fig. 9C) did move southward in association with the upper-level center (fig. 9A). An inspection of daily Northern Hemisphere sea level charts for May also disclosed the predominantly continuous nature of the retrogression of the surface cells.

A complete physical explanation of the unusually persistent retrogression of these mean polar vortices cannot be attempted here. However, a brief study was made of how well the polar trough was predicted by the daily and

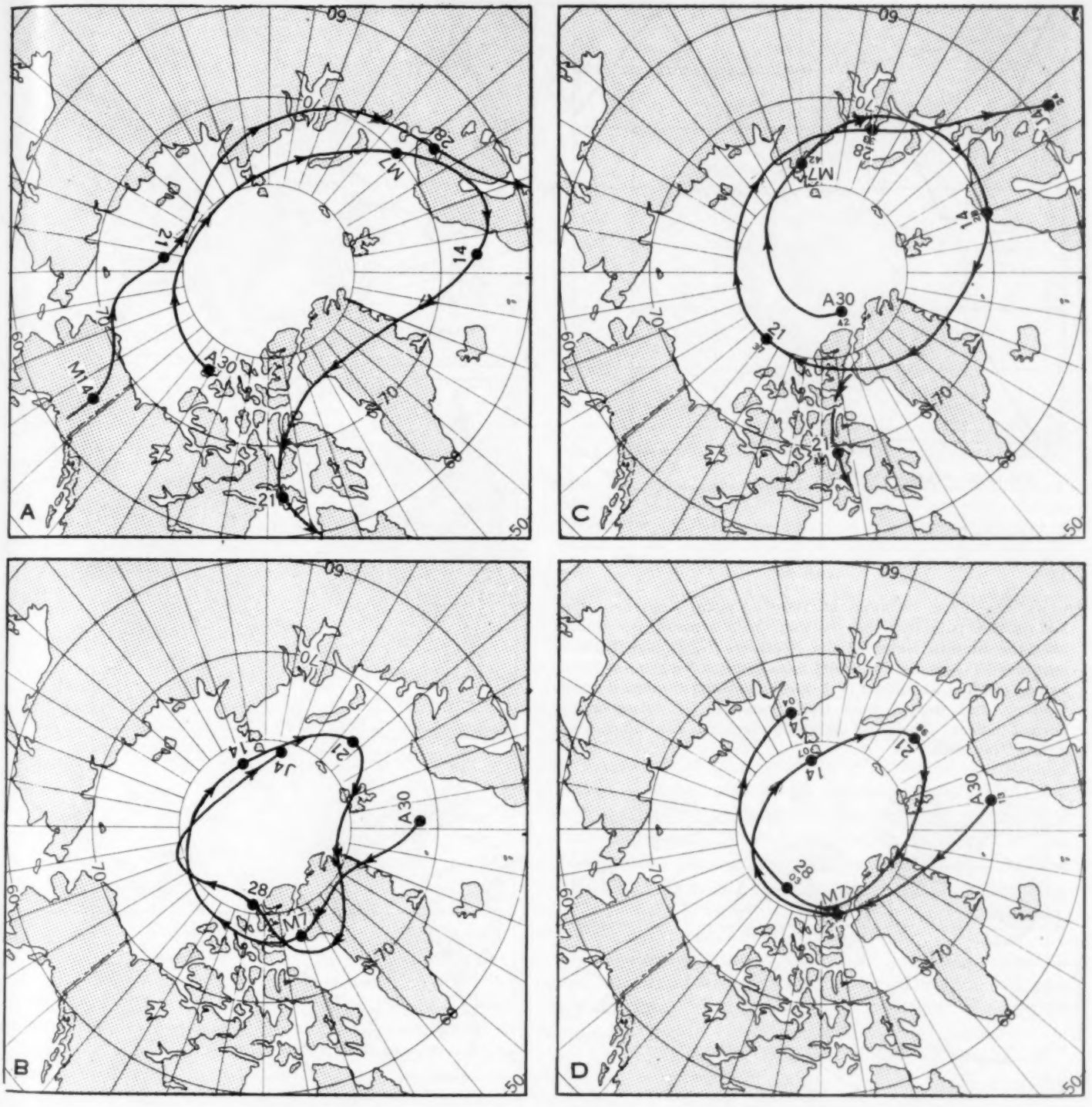


FIGURE 9.—Tracks of 5-day mean polar vortices during May 1960 at 700 mb. for (A) anticyclone, (B) cyclone, and at sea level for (C) anticyclone, (D) cyclone. Top number is middle day of period; lower number on (C) and (D), intensity of center (millibars). Continuous retrogression of high-latitude vortices around the pole was the most unusual circulation feature of May.

5-day mean barotropic charts now in use in the Extended Forecast Section [3]. Results showed that in general the direction of motion (retrogression) was correctly forecast, but the forecast magnitude was only about half the observed motion. This would indicate that the principle of conservation of absolute vorticity was applicable, at least qualitatively.

Variations in the strength of the polar zonal circulation were quite marked as a result of rotation of these systems around the pole. To illustrate this, figure 10 shows the

554818—60——5

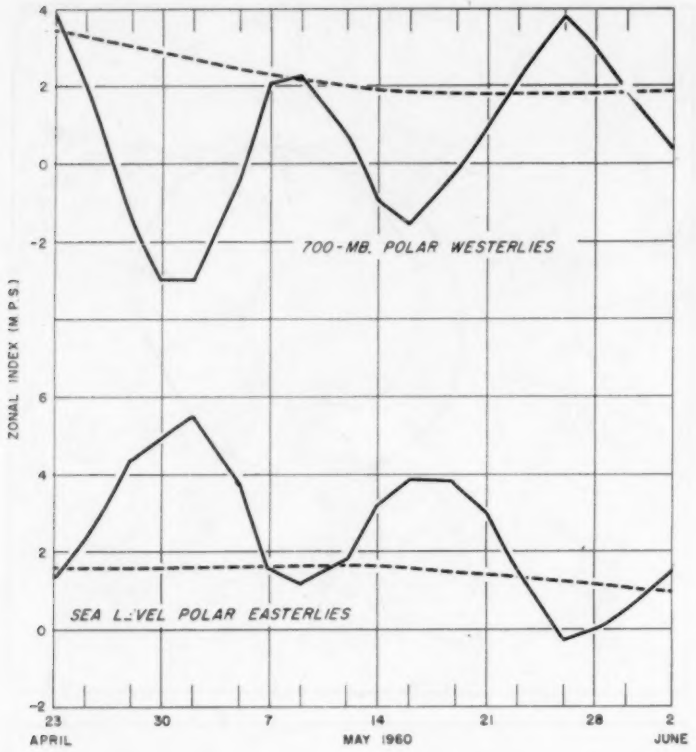


FIGURE 10.—Time variation of 700-mb. polar westerlies (top) and sea level polar easterlies (bottom) (both in meters per second) over the western sector of the Northern Hemisphere between latitudes 55° and 70° N. Solid lines connect 5-day mean index values (plotted at middle of 5-day period and computed thrice weekly), and dashed lines show variation of corresponding normal indices. The polar circulation featured two index cycles during May 1960.

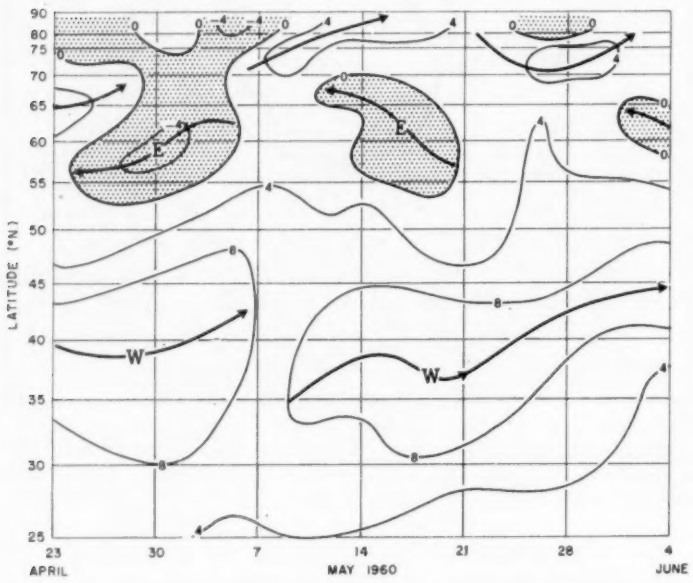


FIGURE 11.—Time-latitude section of 5-day mean zonal wind components at 700 mb. averaged over the western part of the Northern Hemisphere. Isotachs are in meters per second with easterly winds stippled. Primary wind axes (both easterly and westerly) are shown as solid arrows. The alternating periods of net easterly and westerly flow at the higher latitudes reflect the periodicity in the polar circulation.

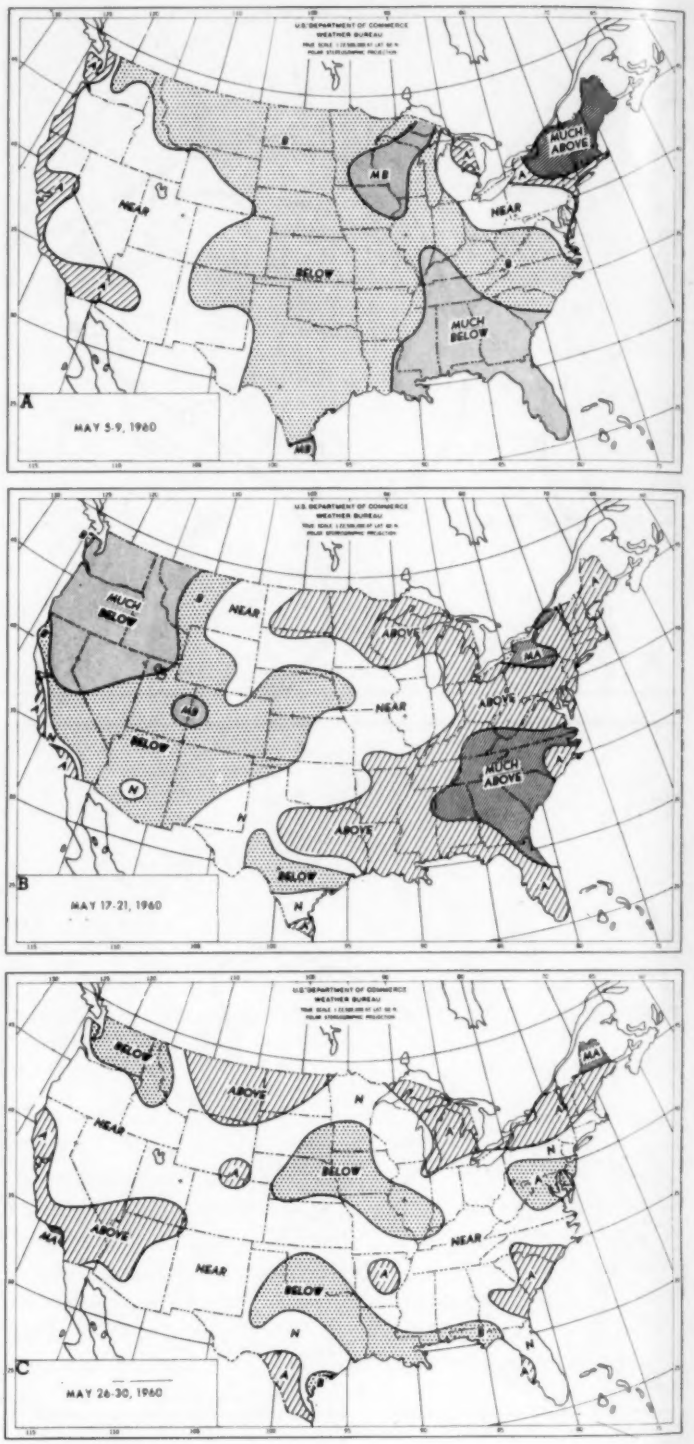


FIGURE 12.—Observed 5-day mean temperature classes over the United States for periods corresponding to those in figure 13.

time variation during May 1960 of the 5-day mean values of 700-mb. polar westerlies and sea level polar easterlies averaged over the western part of the Northern Hemisphere between 55° N. and 70° N. Clearly there were two complete index cycles which were closely related to positions of the sub-polar cells. As an example, note that when the cyclonic vortex occupied the Canadian Arctic

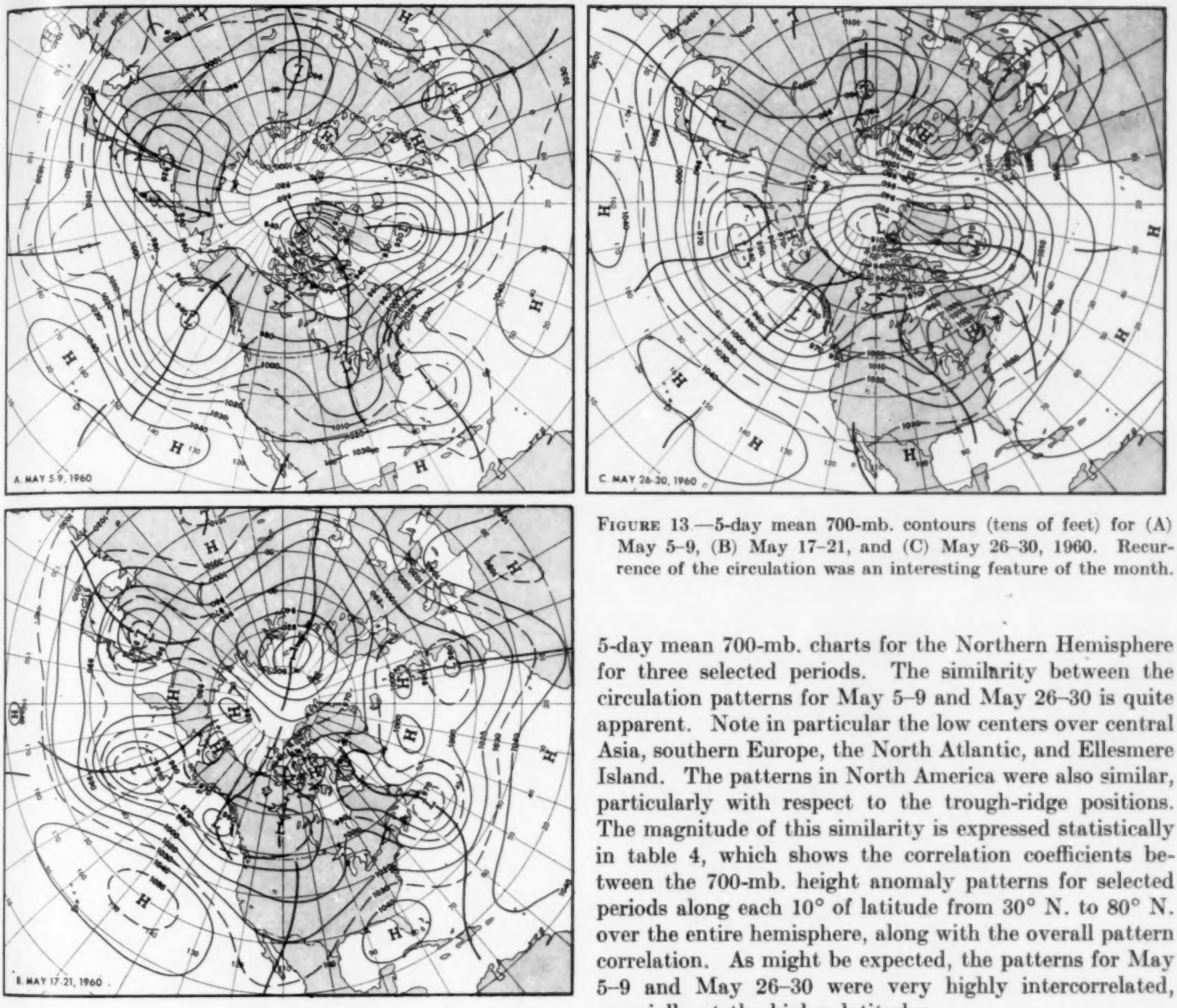


FIGURE 13.—5-day mean 700-mb. contours (tens of feet) for (A) May 5–9, (B) May 17–21, and (C) May 26–30, 1960. Recurrence of the circulation was an interesting feature of the month.

area on the 7th and 28th of May (fig. 9B), the polar westerlies were at a maximum and polar easterlies at a minimum (fig. 10), but the reverse was true when high pressure occupied the same area. The relation between position of the polar cells and the zonal circulation is further illustrated by figure 11, which shows the time-latitude variation of 5-day mean zonal wind speeds averaged over the Northern Hemisphere at 700 mb. The alternating periods of easterly and westerly circulation at the higher latitudes reflect the index cycles previously mentioned.

It is evident that a recurrence of approximately 3 weeks existed in the polar circulation. This was also true of the mid-latitude circulation patterns over much of the hemisphere and of the temperature patterns in the United States (figs. 12 and 13). Figure 13 shows the 5-day mean 700-mb. charts for the Northern Hemisphere for three selected periods. The similarity between the circulation patterns for May 5–9 and May 26–30 is quite apparent. Note in particular the low centers over central Asia, southern Europe, the North Atlantic, and Ellesmere Island. The patterns in North America were also similar, particularly with respect to the trough-ridge positions. The magnitude of this similarity is expressed statistically in table 4, which shows the correlation coefficients between the 700-mb. height anomaly patterns for selected periods along each 10° of latitude from 30° N. to 80° N. over the entire hemisphere, along with the overall pattern correlation. As might be expected, the patterns for May 5–9 and May 26–30 were very highly intercorrelated, especially at the higher latitudes.

On the other hand, the May 17–21 circulation, approximately midway between the two periods cited above, was quite different. While the May 5–9 and May 26–30 periods had strong ridges centered over Scandinavia, the May 17–21 circulation featured a deep sub-polar Low. Other major differences are apparent elsewhere over the hemisphere. Table 4 shows that the latitudinal correla-

TABLE 4.—*Correlation of 5-day mean 700-mb. height anomalies over the Northern Hemisphere between selected periods during May 1960*

| Periods | Latitude (° N.) | | | | | | Overall correlation |
|---|---|---|---|---|---|---|---|
| | 80 | 70 | 60 | 50 | 40 | 30 | |
| May 5–9 and May 26–30 | 0.94 | 0.96 | 0.69 | 0.36 | 0.27 | 0.30 | 0.67 |
| May 5–9 and May 17–21 | −.72 | −.90 | −.27 | .34 | −.41 | .09 | −.22 |
| May 17–21 and May 26–30 | −.86 | −.81 | −.24 | .21 | −.15 | .30 | −.04 |

tions between May 5–9 and May 17–21 were quite similar to those between May 17–21 and May 26–30. At higher latitudes both sets of correlations were very strongly negative.

In order to determine how well this circulation recurrence was reflected in the temperature patterns in the United States (fig. 12), a count was made of the number of stations (out of 100) whose temperature class either remained the same or differed by not more than one class. It was found that 75 percent of the stations satisfied this condition for the similar circulation patterns, May 5–9 and May 26–30. However, a count between May 17–21 and each of the two periods May 5–9 and May 26–30 gave percentages of only 53 and 69, respectively. Although other factors are involved, it would appear, then, that the temperature patterns in the United States were related, in part, to the concomitant circulation changes over the polar regions.

## REFERENCES

1. U.S. Weather Bureau, *Weekly Weather and Crop Bulletin, National Summary*, vol. XLVII, No. 23, June 6, 1960.
2. J. F. O'Connor, "The Weather and Circulation of April, 1960—A Sharp Mid-Month Drop in the Zonal Westerlies Accompanied by a Temperature Reversal in the Contiguous United States," *Monthly Weather Review*, vol. 88, No. 4, April 1960, pp. 158–166.
3. J. Namias and Collaborators, "Application of Numerical Methods to Extended Forecasting Practices in the U.S. Weather Bureau," *Monthly Weather Review*, vol. 86, No. 12, Dec. 1958, pp. 467–476.

U.S. GOVERNMENT PRINTING OFFICE: 1960